An A15 Conductor Design and its Implications for the NET-II TF Coils

Final Study Report

R. Flükiger, F. Arendt, A. Hofmann, U. Jeske, K. P. Jüngst
P. Komarek, H. Krauth, W. Lehmann, J. Lühning, B. Manes
W. Maurer, A. Nyilas, W. Specking, P. Turowski and H. Zehlein
Institut für Technische Physik

Kernforschungszentrum Karlsruhe

KERNFORSCHUNGSZENTRUM KARLSRUHE

Institut für Technische Physik

KfK 3937

An A15 Conductor Design and its Implications for the NET-II TF Coils

Final Study Report

by

R. Flükiger, F. Arendt, A. Hofmann, U. Jeske, K. P. Jüngst, P. Komarek,
H. Krauth, W. Lehmann, J. Lühning, B. Manes, W. Maurer, A. Nyilas,
W. Specking, P. Turowski, and H. Zehlein

Abstract

The paper describes the results of studies for a NET toroidal field coil
conductor carried out at KfK-Karlsruhe. The conductor concept is based on
the same design principles as used in the Euratom-LCT coil, well proven in
all conductor tests and the domestic tests of the coil. These principles are
applied to the peculiarities of Nb_3Sn for a rated current of 20 kA at 12 T,
taking into account ac losses and nuclear heating. A flat Nb_3Sn cable is
soldered to a surrounding CuNi tape after reaction. Around this rectangular
conductor core, Cu profiles are cabled on distance by the Roebel-process and
subsequently soldered onto the CuNi tape. The whole system is surrounded by
a steel conduit.
The conductor data result from electric, thermohydraulic and stability cal-
culations as well as mechanical evaluations. Expected fabrication processes
are discussed, and measurements on a first simplified subsize conductor mo-
del are presented.

Ein A15 Leiterkonzept für NET-II Toroidalfeldspulen

Zusammenfassung

Die vorliegende Arbeit beschreibt eine Studie über einen Leiter für NET-
Toroidalfeldspulen, die am KfK Karlsruhe durchgeführt wurde. Das Leiterkon-
zept beruht auf denselben Konstruktionsprinzipien, die schon bei der LCT-
Spule angewendet wurden und alle Leitertests sowie den LCT-Spulentest er-
folgreich bestanden haben. Diese Prinzipien wurden den besonderen Material-
eigenschaften von Nb_3Sn angepaßt, für Ströme von 20 kA bei 12 T, unter Be-
rücksichtigung der Wechselstromverluste und der nuklearen Heizung. Ein fla-
ches Nb_3Sn-Kabel wird nach der Reaktion in eine CuNi-Hülle eingelötet. Um
diesen rechteckigen Leiterkern werden Kupferprofile verröbelt und nachträg-
lich auf die CuNi-Hülle aufgelötet. Das ganze System wird noch von einem
Stahlmantel umhüllt.
Die technischen Leiterdaten wurden aus Berechnungen des elektrischen und
thermohydraulischen Verhaltens unter Stabilitätsbedingungen berechnet, er-
gänzt durch mechanische Analysen. Die zu erwartenden Fabrikationsprozesse
werden besprochen, und Messungen an einem ersten vereinfachten Leitermodell
in reduziertem Maßstab werden vorgestellt.

1. Introduction

The use of A15 conductors for the NET TF coils implies sufficient confidence in the use of these materials, based on previous experimental work. Meeting this goal is expected after increasing success of the development programmes under progress now. On the other hand, the information available so far is too incomplete to provide satisfactory input data for the conceptual NET coil design. This study represents therefore a first evaluation rather than a final design of the conductors to be used in NET later on. Thus, modifications based on the further development progress can be expected until the final NET design will start.

Starting point for this study was the information collected in the previous INTOR /1/ studies, the practical experiences in the development of superconducting magnets, especially with the Euratom LCT coil and the progress reached so far in the Euratom Programme task M3 ("Development of High Field Composite Conductors").

As boundary conditions, the NET-II parameters have been used. Following informations provided by the NET team have been taken into account:

- the coil definition given in the note from February 2, 1984,
- the operation scenario given in the note from March 23, 1984,
- the preliminary stress analysis results given in the note from March 23, 1984,
- the transient field distribution across the TF coils calculated by N. Mitchell,
- the calculation of field and force distribution by M.V. Ricci,
- the neutronic calculations for heat and radiation energy deposition by W. Daenner (NET/IN/84-067, 26.7.84).

The main data of these informations and additional calculations which have been performed are described in the appropriate chapters.

Starting point was the design principle previously chosen for the conductor of the EuratomLCT coil. This is very well justified by the successful test of this coil in the TOSKA /14/ test facility in Karlsruhe and the stability tests for the conductor. Thus, the attempt has been made to keep the principles also for the A15 NET-conductor design. These principles are

- forced flow cooling for
  -- ensured electrical insulation,
  -- effective force transmission,
  -- predictable thermohydraulics,
  -- simplified winding fabrication;

- large wetted perimeter for a given hydraulic diameter to provide optimal stability,
- mechanically fixed conductor strands to avoid disturbance energy created by mechanical movement,
- strand separation or resistive barriers for reducing ac losses,
- steel reinforcement for force transmission and support of the large hoop stresses.

The conductor design proposed in the earlier INTOR studies /1/ was already based on these principles. As it will be explained in chapter 2.1, further investigations indicate that it might be rather difficult to develop an economic fabrication process for this conductor. Thus, it was concluded to propose a modified conductor concept, still based on the above mentioned LCT experience. This conductor concept will be described in the following together with options for the fabrication processes which will need to be investigated further. The calculations leading to the present conductor concept and its dimensions are reported.

Based on the experimental results in the M3 task, two issues can be concluded, namely the strand optimization and the influence of steel reinforcement on the electrical data of the conductor. As will be summarized briefly in chapter 6, the work on ternary alloying of Nb_3Sn showed the following results:

- The strain related current density degradation is physically well
  understood and can be reduced by ternary alloying,
- an increase of critical current is mainly of importance at high
  fields (B $>$ 11 T) and is related to an increase of the upper
  critical field, B_{c2},
- quantitative improvements are practically independent of the kind
  of ternary additions (Ti, Ta, Zn, ...).

Concerning steel reinforcement prior to reaction, the investigation
of several alloys showed that by use of Incoloy-type (series 900)
materials, perhaps in combination with molybdenum, optimal matching
of the prestrain is possible. These results are taken into account
for the present conductor design.

As a special item in the study contract, the problem of radiation
damage in magnets, especially in the superconductors stabilizing
materials and the insulation, has been treated. A survey on the
present state of the art has been carried out. It will be summarized
briefly in chapter 3.4 and is published in full length in two special
reports.

2. The NET-II/KfK Conductor Design

2.1. Influence of the LCT experience for the conductor design

2.1.1 LCT design principles

Based on the experiences during the LCT project several issues are
seen justifying to keep as much as possible the design principles
also for NET. These principles are already listed in chapter 1. The
experiences obtained above concern structural materials, conductor
behavior, fabrication steps, handling of reacted conductors, cooling
of large masses and coil stability behavior.

2.1.2 The fabrication experiences

The fabrication development of the LCT conductor provided information
on the following processing steps:

- the Roebel technique for cabling of strands to a flat cable with
  free space between the strands for He flow,
- soldering of a Roebel cable, just on the bottom of the strands, to
  a solder cladded steel core,
- the wrapping up of the conductor with a steel conduit, welded
  He-tight along the whole conductor length.

These techniques have been developed for 1000 m conductor unit
length. In addition, the inspection and quality assurance methods
(seee chap. 5.5) have been developed to a satisfactory level.

2.1.3 Experimental conductor and coil behaviour

Measurements on long length samples of the conductor were carried out
for testing the electric, mechanical and thermohydraulics behaviour.
By these results all calculation principles have been verified, as
e.g. in the HELITEX experiment /2/ all thermohydraulics data have
been provided. Major emphasis was given to stability measurements,
first on long length samples and finally at the single-coil tests in
the KfK facility TOSKA.
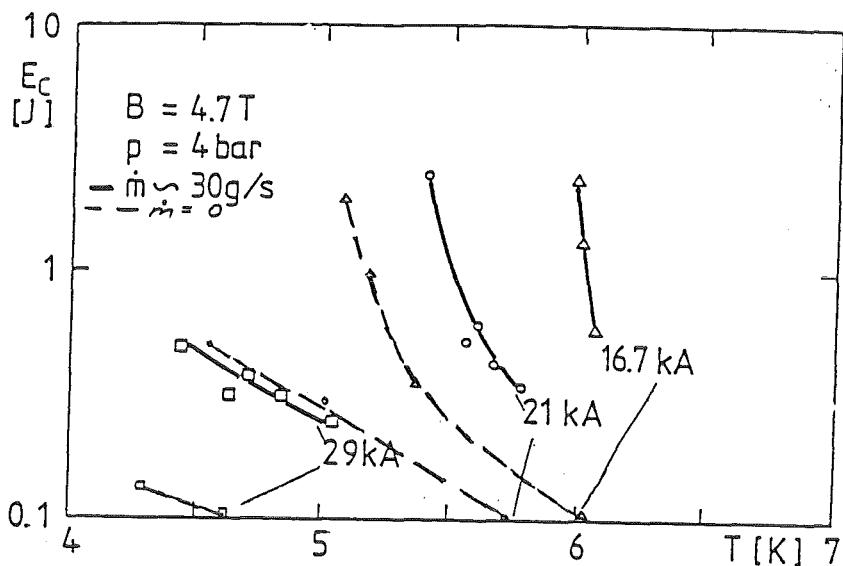
Fig. 2.1-1: Example for stability measurements on the Euratom-LCT-
conductor: Critical energy E_c for localized transients
(5 cm long heater) as a function of He inlet temperature,
for different conductor currents at 4,7 T. The difference
between high He mass flow rate ($\dot{m}$ = 30 g/s) and stagnant
He ($\dot{m}$ = 0) is shown.

Fig. 2.1-1 shows for example the stability measurements carried out on a 3 m long conductor piece in the W7 conductor test facility /3/. The critical energies for localized transients (about 5 cm length) at different currents, without and with high He-mass flow through the conductor, are plotted versus the He-inlet temperature. The curve for 29 kA is comparable to the conditions in the coil ($\sim$8 T, $\sim$4 K), indicating a critical energy of about 1 J at 4 K, equivalent to 100 mJ/cm^3 for the given experimental arrangement. This is the value envisaged in the design. As shown by the coil measurements, the actual disturbance level is certainly much smaller. Fig. 2.1-2 shows the main stability results /4/. The He mass flow rate was kept very small (12 % of the rated one) and the helium was heated up to 5.8 K at the conductor inlet of one double pancake. Under these severe conditions the coil was charged, operated and fast dumped without deterioration of performance or stability. If one indicates the as a
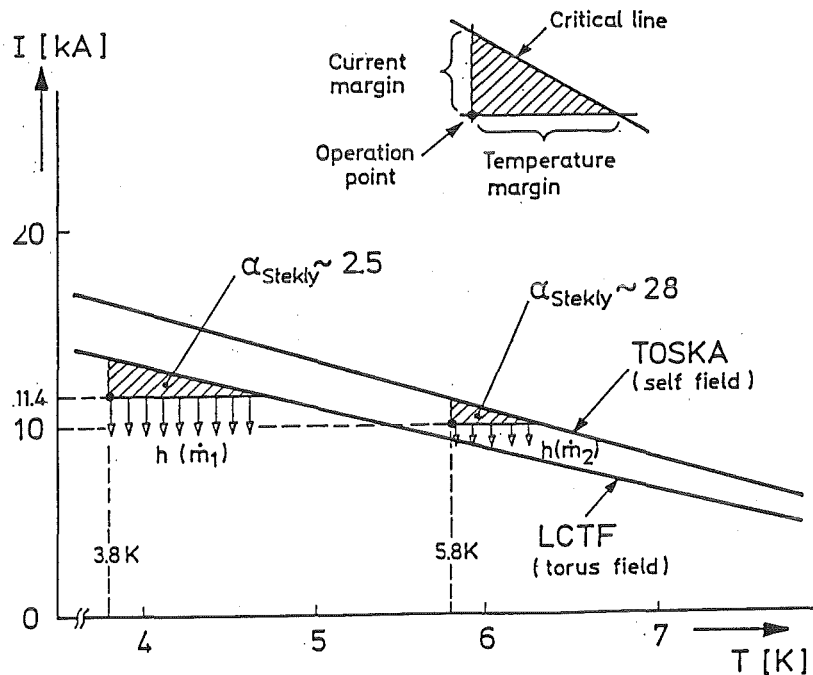
Fig. 2.1-2: Stability margin of the EURATOM LCT-coil, based on mea-
surements in the TOSKA facility. With a He inlet tempera-
ture of 5,8 K and only 12 % of rated mass flow m_1 (m_2 =
1,2 g/s) the coil remained superconducting in a fast dis-
charge, in spite of the stability parameter α_{stekly} = 28
for these conditions. The stability margin as expected in
the LCTF-tests is also shown (The value of 11.4.kA
corresponds to the rated current in the LCTF).

remaining stability margin for this operation in a I_c (T)-diagramme as a triangle (shown in Fig. 2.1-2) and takes into account the heat transfer coefficient of only 0.015 W/cm^2 K (due to the small mass flow rate of 1.2 g He/s) a Stekly stability parameter α of about 28 will result. Thus, the coil could be operated far below "cryogenic" stability, indicating very small disturbance levels. Such small levels could certainly only be provided by a rigid winding and coil construction, only possible with forced flow conductors. For comparison, Fig. 2.1-2 also indicates the available stability margin for the tests at ORNL, which is a factor of about 9 higher due to the conditions on current, field temperature and mass flow, thus providing sufficient margin for ac loss heating and extended performance conditions.

2.1.4 <u>Reasons for changing the concept since INTOR</u>

As mentioned above, the Roebel process has been found as the only suitable one for cabling of NbTi strands on distance to a flat cable. As an extension the preliminary INTOR conductor design was thus based on a Roebel process of the Nb$_3$Sn strands. The direct transfer of the LCT Roebel technique to Nb$_3$Sn/CuSn strands has been analyzed now. The mechanical processing of a bronze type matrix is quite different from a copper matrix system. High bending forces are in general necessary to bend a strand with a given geometry to a required precise position. The high yield strength of the bronze matrix leads to a high mechanical resistance against any deformation.

Table 2.1-1 summarizes the mechanical properties of Cu-Sn bronzes at various temperatures. According to the data of this table, for an achievement of similar fabrication conditions as in the case of LCT cable fabrication (e.g. necessary bending forces of the strands), the Roebel head should be processed at at least 400° C. The necessary accurate process temperature must be determined by prior tests. Processing of the Roebel head at about 400° C will cause numerous difficulties which must be solved prior to cable manufacturing, too. These problems are :

- The Roebel system should be processed at inert environment and at about 400° C,

- remote control of the adjustment system for the punching tools during cabling,

Materials	Yield strength (MPa)	Ultimate tensile strength (MPa)
LCT strand	350	400
Cu-10 Sn Bronze*)		
half-hard at ambient	420	580
hard at ambient	553	700
hard at 250°C		658
hard at 300°C		612
hard at 350°C		532
hard at 400°C		451
hard at 500°C		168
Cu-13.5 Sn Bronze **)		
40% areal reduction ambient	800	820
Heat treated 500°C/90 min ambient	400	580
Heat treated 700°C/64 hrs. ambient	165	261

*) Copper data sheets /5/
**) Measurements at KfK

Table 2.1-1: The mechanical properties of different bronze materials at various temperatures.

- sticking of copper-tin dust in the sensitive tool region of the head,

- unknown problems by creep of the tool materials at this temperature (a continuous process would be vulnerable),

- for the development of a new Roebel system full cable lengths should be tested (at least with dummy Cu-13Sn strands) to avoid any misleading information due to short lengths.

According to the above mentioned points the application of Roebel cabling to a Nb_3Sn type bronze matrix conductor needs necessarily the development of such a new Roebel head.

Therefore, the actual feasibility of a continuous Roebel process for $Nb_3Sn/Cu-Sn$ strands cannot be guaranteed. This requires the development of a new conductor concept described in the following chapters. It will be shown later on that the Roebel process will nevertheless be used in the NET-II/KfK concept, but for the Cu stabilization profiles only, the Nb_3Sn strands being cabled.

2.2 General description of the NET-II/KfK conductor

The NET-II/KfK conductor concept, designed for taking into account nuclear heat as well as the ac losses induced by the poloidal fields is represented in Fig. 2.2-1. The forced flow cooled conductor consists of:

- a core comprising 36 Nb_3Sn strands of 1.92 mm diameter, wound around a thin insulating strip, calibrated and confined by a CuNi electrical barrier,
- a cryostabilizing region composed of 26 Cu rectangular profiles separated from each other by He channels,
- an external steel conduit,
- an insulator layer.
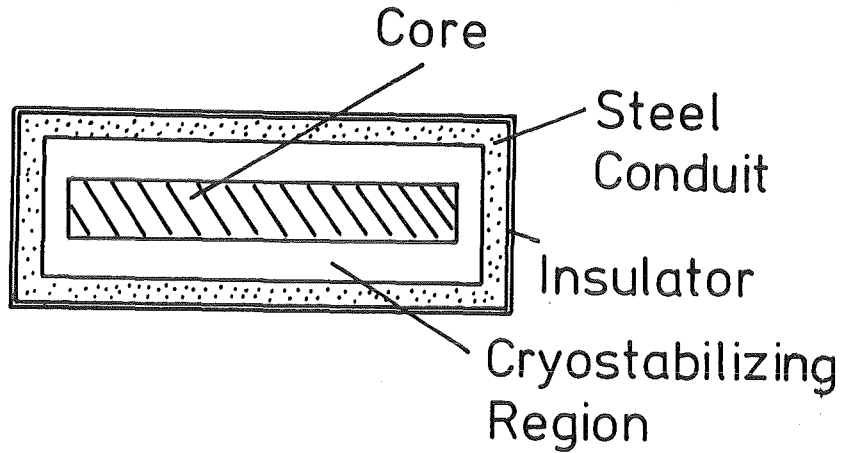
Fig. 2.2-1: Schematic representation of the NET-II/KfK-conductor

2.2.1   The core

The core is composed of 36 Nb_3Sn bronze processed strands of 1.92 mm diameter, wound around a folded insulating strip (a thin Cu-Sn bronze foil folded around an insulating ribbon, woven with very thin ceramic fibres) of 0.5 mm thickness, which are enclosed in a CuNi barrier. The Nb_3Sn strands have an internal Cu stabilization, separated from the bronze by a Ta barrier. The external part of the wire consists of bronze, thus enhancing the electrical resistance between the Nb_3Sn filaments of two neighbouring strands, which are characterized in Table 2.2-1.

Superconducting material	Nb_3Sn (or $(Nb\text{-}7Ta)_3Sn$)
External diameter (mm)	1.92
Bronze: Nb ratio	3.1:1
Cu	23%
Ta	4%
number of filaments in one strand	$\sim$56 000
filament size (μm)	$\sim$ 4
twist pitch (mm)	50
J_c (non copper) at 12 T/4.2 K (A/cm^2)	4.2×10^4
J_c (overall) at 12 T/4.2 K (A/cm^2)	3.1×10^4

Table 2.2-1: Characterization of Nb_3Sn strands

After being wound with a transposition length of 330 mm around the insulation strip, the Nb_3Sn strands are calibrated to the dimension 36.0x4.1 mm^2. Due to this very flat conductor design, the maximum bending strain on the Nb_3Sn strands will not exceed 0.13%, even at the smallest curvature of the NET-II coil, r $\sim$ 1500 mm (see 3.3). After calibration, the strands will not longer have a round shape but will be compressed to a thickness of 1,8 mm (see Fig. 2.2-2), thus allowing a distance of 0.1 mm between the calibrated Nb_3Sn strands and the CuNi barrier. This thickness has to be kept as low as possible, in order to maintain the electrical resistance between the Nb_3Sn strands as high as possible. A solder material with $\rho = 1.6 \times 10^{-8}$ Ωm will be chosen.
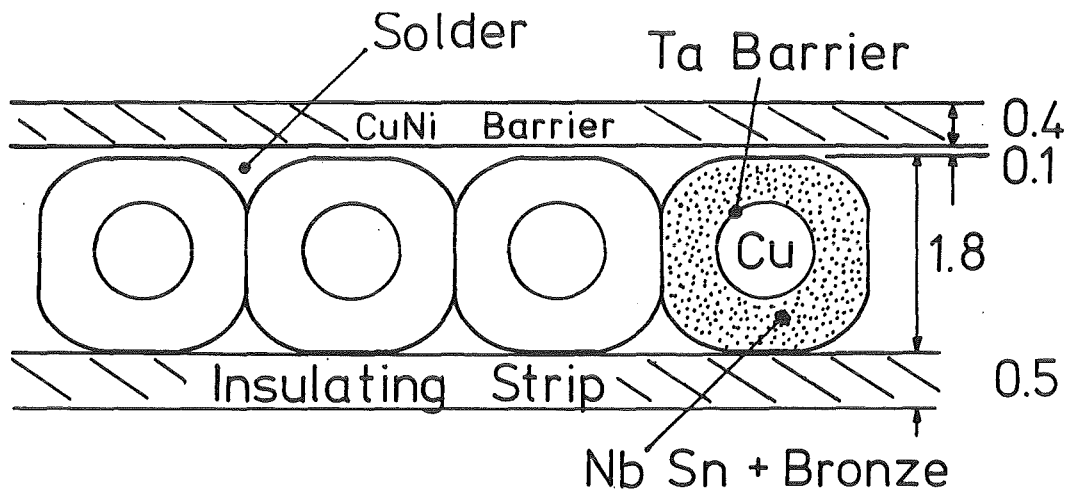
Fig. 2.2-2: Geometrical arrangement of calibrated Nb_3Sn strands in the core. The internal Cu stabilization (23% Cu) and the Ta barrier are shown.

The soldering of the CuNi barrier and the calibrated Nb_3Sn strands occurs <u>after</u> the reaction heat treatment. It should be mentioned that after calibration, a certain amount of voids ($\sim$5-8 mm^2) at the inside of the core (between the strands and the insulating strip) will subsist. The latter are not considered as being relevant, due to their geometrical location. If necessary, this void cross section could be lowered to $\sim$2 mm^2 by further deforming the Nb_3Sn strands to a thickness of $\sim$1.7 mm. An alternative approach would consist of assembling the whole core, i.e. insulation strip, Nb_3Sn strands and CuNi barrier, <u>prior</u> to the reaction heat treatment. This would have the advantage of avoiding the soldering procedure, but the intimate contact between the calibrated Nb_3Sn strands and the CuNi barrier would be more problematic. At the present state of knowledge, preference should thus be given to the first solution.

2.2.2 Cu stabilizer and He channels

Following the principle of using He channels as perfect electric insulating barriers between Cu stabilizers, the cryostabilizer section is formed by 26 Cu profiles of rectangular cross section (3.6x2.2 mm^2), separated by the channels each 1 mm wide (see Fig. 2.2-3). The Cu profiles must fulfill the following requirements:

a) they consist of high conductivity copper with sufficient mechanical strength for transmitting the transverse mechanical stresses of 55 MPa (Fig. 3.3-1) without being mechanically deformed,

b) they have to be soldered to the core (more precisely to the Cu-Ni) in order to ensure current and heat transfer. A high quality soldering process is required in order to avoid both, mechanical movements during operation and contact between two neighbouring Cu profiles. The latter could eventually lead to the blocking of He channels: the situation can be eased by cutting small slots of 1x1 mm^2 on the narrow face of the Cu profiles after each few meters,

c) the rugosity of the wetted Cu profile surfaces should be increased by mechanical procedures, thus increasing the total cooling surface,

Cu Profiles, 3.6×2.2, 24% Nb$_3$Sn strands
ϕ1.92×36, 12%
Steel Conduit, 33%
Insulation, 8 %
He channels
3.6×1.0, 13%
CuNi Barrier, 4%
Folded Strip, 2%

2.45
0.5
18.2
12.3
5.1
0.4
0.5

37.0
2.45
41.4
0.5
47.3

Fig. 2.2-3: The NET-II/KfK conductor
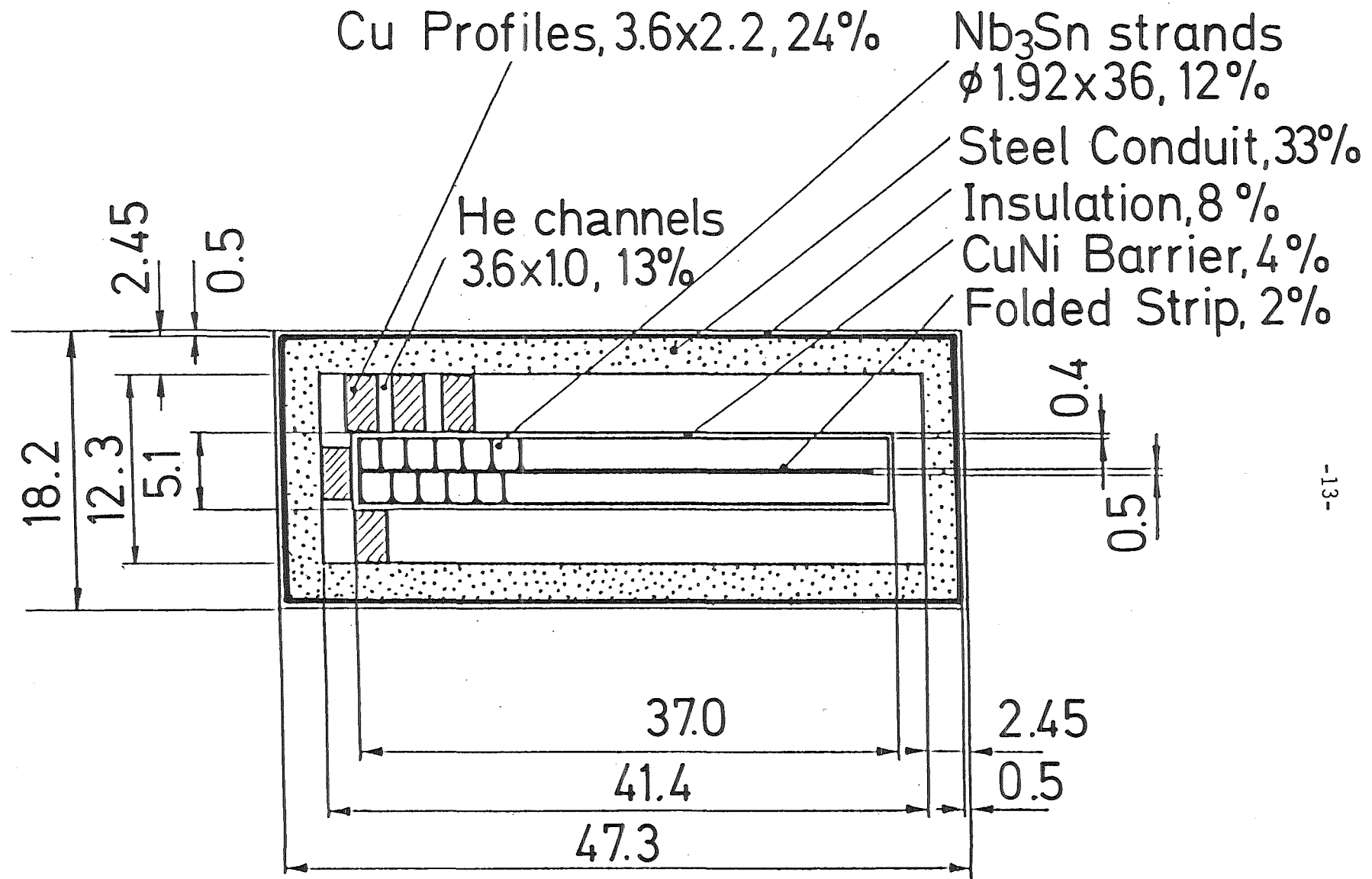
d)   The forces acting on the core during the operation of mounting the Cu
       profiles on the core must be minimized for preventing any damages to
       the Nb_3Sn strands. This is accomplished by using the Roebel techni-
       que, previously employed for the construction of the Euratom-LCT
       coil.

e)   The Roebel process inherently comprises the risk of contacts between
       two neighbouring Cu profiles at the corners of the core, which would
       seriously enhance ac losses. This can be avoided by choosing an
       appropriate transposition length for the Cu profiles, i.e. around
       1 m /6/. An alternative would consist in mounting the Cu profiles
       parallel to the conductor axis: This would of course be somewhat
       easier than the Roebel technique, which, however, has a considerable
       advantage: with a transposition length of 1 m, the Cu profiles are
       automatically kept in place after each half turn around the core,
       i.e. all $\sim$ 40 cm. This causes an excellent lateral anchorage of the
       Cu profiles, which could never be obtained if the latter were
       parallel.

2.2.3   The steel conduit

The steel conduit has several functions:

- to provide a vacuum-tight enclosure for the flowing He,
- to withstand the hoop stresses due to Lorentz forces, maintaining
  the strain during operation around 0.2%,
- to transmit (partly) the radial forces towards the central vault in
  the 16 coil assembly
- to avoid mechanical movements during operation,
- to withstand the high He pressures (> 100 bar) developed after a
  possible quench.

A particular care must be given to the assembling of the core with
roebled Cu profiles and the steel conduit, which must occur without
any irreversible damage for the superconducting strands. The required
absence of forces between steel conduit and Nb_3Sn strands in the
mounting phase excludes

- any subsequent calibration step,
- any one-step wrapping procedure of the type used for the NbTi
  Euratom LCT-coil.

In the present design, preference has thus been given to a steel coßduit formed by 4 tapes of 2.45 mm thickness, which are brought in position around the Cu profiles and then laser-beam welded at the 4 corners (see section 5.3).

2.2.4 The insulation

The insulation consists of tapes of polyimides (PG-10CR), which are wrapped around the steel conduit up to the thickness of 0.5 mm. Between two adjacent conductors, the total distance of 1 mm is considered to be sufficient for preventing electric arcs due to the high voltage (PG-10CR is able to withstand breakdown voltages of several tens of kV per mm). The mechanical behavior of such an insulation under irradiation is described in 3.4.

2.3 Characteristic data for NET-II/KfK conductor

	(mm^2)	(%)
Total Cross Section: 47.3 x 18.2	861	100
Nb$_3$Sn + bronze, 36 x Ø1.92 (without the 23% stabilizing Cu)	76	8.8
Cu, in the strands	24 ⎫	
Cu profiles 26x(3.6x2.2)	206 ⎭	26.7
Ta	4	0.5
He channels	115	13.3
Folded strip (32.4 x 0.5)	16	1.9
CuNi barriers	33	3.8
Steel conduit	287	33.4
Insulation	65	7.5
Solder + voids	35	4.1

Table 2.3-1: Characteristic geometry data for NET-II/KfK conductor

Table 2.3-2: Summary of NET-II/KfK conductor characteristics

Conductor	Units	
Core		
Strand		
Superconducting material		Nb_3Sn (or $(Nb-7Ta)_3Sn$)
Processing		Bronze process
Number of strands		36
Strand diameter	mm	1.92
Bronze/Nb ratio		3.1 : 1
Stabilization of strands		internal Cu (23%), separated from the bronze by a Ta (4%) barrier
Number of filaments in strand		$\sim$ 56.000
Size of filament	μm	$\sim$ 4
Twist pitch	mm	50
J_c (non copper) at 12 T/4.2 K	A/cm^2	4.2×10^4
J_c (overall strand) at 12 T/4.2 K	A/cm^2	3.1×10^4
Transposition length of strands around strip	mm	330
Strip		
Thickness of folded insulating strip	mm	0.5
Materials and arrangement of strip		Cu-Sn bronze foil folded around an insulating ribbon woven with very thin ceramic fibres
Cable		
Dimensions of core after calibration	mm x mm	36.0 x 4.1
Solder material		Bi alloyed Sn solder
Barrier material		CuNi
Barrier thickness	mm	0.4

Table 2.3-2: continued

	Units	
Cryostability region		
<u>Stabilizer</u>		
Material		Cu profiles (half-hard)
RRR		150
Profile dimensions	mm x mm	3.6 x 2.2 (with slots
		($\sim$0.5 mm) for He passage
Distance between profiles	mm	1.0
Transposition length	m	1.0
Solder material		Bi alloyed Sn solder
<u>Cooling channels</u>		
Dimensions	mm x mm	3.6 x 1.0
Reinforcing material		316LN
Arrangement		conduit
Thickness	mm	2.45
Fabrication		Laser tack welded
Insulator material		PG-10CR
Insulator thickness	mm	0.5
Conductor properties		
Critical current	kA	30 (at 4.2 K and 12 T)
Operational current	kA	19.85
Total cross section of conductor	mm x mm	47.3 x 18.2 = 861

Table 2.3-3: Coil characteristics with NET II/KfK-conductor

TF Coil

Number of TF coils		16
Operat. current density	kA/cm^2	2.305
Total current per coil	MA	7.938
Axial coil width	m	0.757
Radial coil thickness	m	0.455
Mean winding length	m	25.56
Winding volume per coil	m^3	8.8
Length of inner winding	m	24.08
Kind of winding		double pancake
Number of pancakes per coil		16
Number of turns per pancake		25
Length of conductor per pancake	m	650
X-coordinate of coil center line	m	2.27
X-coordinate of windig facing the plasma	m	2.495
AC-losses per pancake	W	23.4
Nuclear heat per pancake	W	31.2
Static losses per pancake	W	10
Flow losses per pancake	W	15
Additional static losses per coil casing	W	140
Bulk helium temperature	K	4.7 ... 6.2
Helium mass flow per pancake	g/s	5
Initial helium pressure	bar	6
Pressure drop	bar	3.1
Peak heat flux into He	W/cm^2	0.5
Conductor strain due to hoop stresses		$< 2.5 \times 10^{-3}$

3. Design procedure

3.1 Critical current density

The present concept is based on a critical current value of 30 kA at 12 T and 4.2 K, the operating current being 20 kA. The Nb_3Sn strands used for this study are produced by the bronze route. At 12 T, a non-copper current density of 4.2×10^4 A/cm^2 is used, which can be guaranteed by the industry. The average core current density of 31 A/cm^2 leads to a conductor critical current of 46 kA at 12 T and 4.2 K. This provides sufficient safety with respect to possible additional effects, such as transverse mechanical loading or slight strand damage during the fabrication and winding process. In the following a guaranteed critical current of 30 kA is assumed. The variation of J_c with the magnetic field is represented in Fig. 3.1-1.
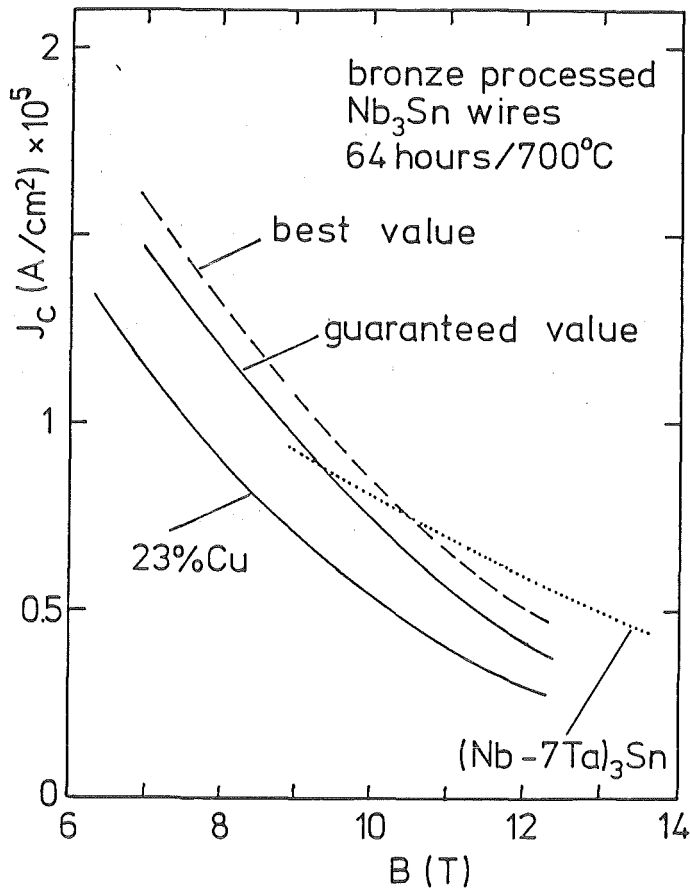
Fig. 3.1-1: J_c vs. B for binary bronze processed Nb_3Sn strands. J_c represents the values without and with the 23% internal Cu, respectively.

At the highest fields in the coil, $\sim$ 11 T, the critical current density of binary Nb_3Sn wires is just equal to that of Ta alloyed Nb_3Sn wires, while at lower fields, J_c of binary Nb_3Sn is higher. At present, it cannot definitively be said whether preference should be given to binary or alloyed Nb_3Sn wires, the final decision being influenced by the state of prestress acting in the conductor. This will only be known after the first measurements on small-scale conductors having the same or a very similar configuration to the NET-II/KfK design. Since both, binary as well as alloyed Nb_3Sn can be produced industrially by the bronze route at comparable costs, the decision can easily be postponed to a later stage when complete stability calculations are available.

3.2   Field distribution

The KfK-conductor concept aims at an internally cooled conductor for pancake windings. In its design, advantage can be taken of the decrease of peak field from the inner to the outer layers of the pancake, which corresponds to enhanced critical and current sharing temperatures and reduced magnetoresistance in the stabilizing copper. For the conservative design of a single type of conductor, in which no grading of material composition is foreseen in any direction, the radial decrease of the maximum field B encountered around the peri-meter and along the azimuthal extent of a coil layer must be used (Fig. 3.2-1):

$$\hat{B}(r') = \max \; B(r' = \text{const.}, y, \varphi) \; , \; \text{where}$$
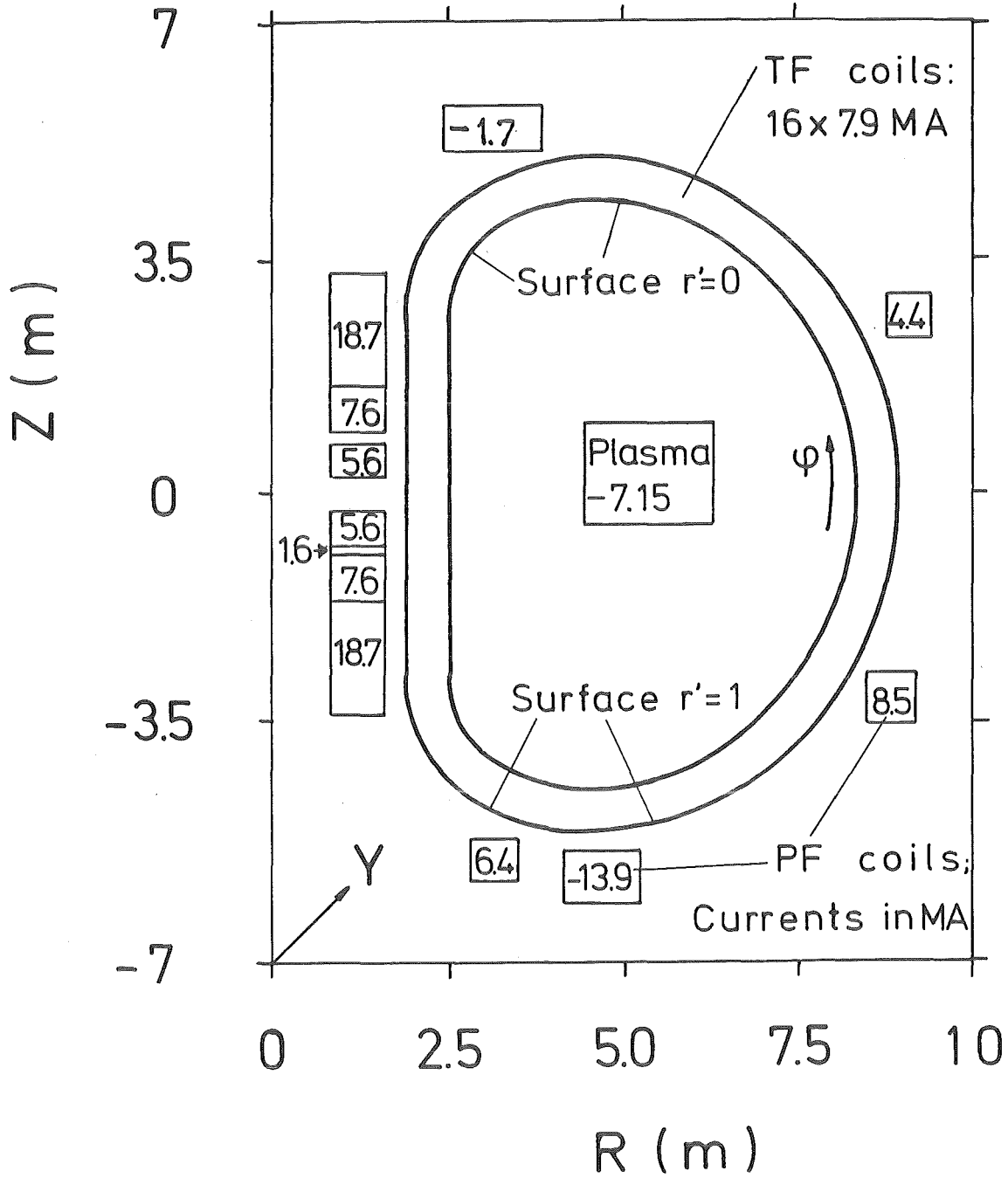
Fig. 3.2-1: Coil and current setup for calculating peak fields in the TFcoil
layers $0 \leqslant r' \leqslant 1$. The PF currents are taken at the end of burn
in the NET II single null divertor case.

r´ measures the radial position of a layer in the winding with r´= 0 at the inner surface of a TF coil (facing the plasma), and r´= 1 at the outer surface. The field values were calculated with EFFI /28/ for 16 identical TF coils and a set of PF coils approximating the Single Null Divertor configuration of NET-II (Fig. 3.2-1) with currents at the end of burn. Fig. 3.2-2 shows $\hat{B}(r´)$ for two variations of TF coils:

a)   Cross section of $\triangle y$ = 70 cm by $\triangle r´$= 63 cm at $\langle j \rangle$ = 1,8 kA/cm^2;

b)   Cross section of $\triangle y$ = 71.3 cm by $\triangle r´$= 46.6 cm
        at $\langle j \rangle$ = 2.4 kA/cm^2.

The radial position of the inner face of the straight leg is at R = 2.495 m in both cases. Case b) is very similar to the reference coil case with the proposed NET II/KfK conductor.

$\hat{B}$ decreases strongly with r´ as long as the peak field occurs in the central pancake of the TF coil, flattening off to an almost constant level when $\hat{B}$ occurs in the edge pancakes at higher r´. In this region, the further decrease of the toroidal field is offset by an increase of the PF components. It is not expected that the picture would change significantly if the PF coils were moved closer to the plasma in case of the radially thinner coil.

For further design work, two straight lines are used to approximate the field dependence shown in Fig. 3.2-2:

$$\hat{B}(r´)\ [T] = \begin{cases} 10.7 - 7.9\ r´ & \text{for } 0 \leq r´ \leq .59 \\[2mm] 6.5 - 0.8\ r´ & \text{for } .59 \leq r´ \leq 1. \end{cases}$$
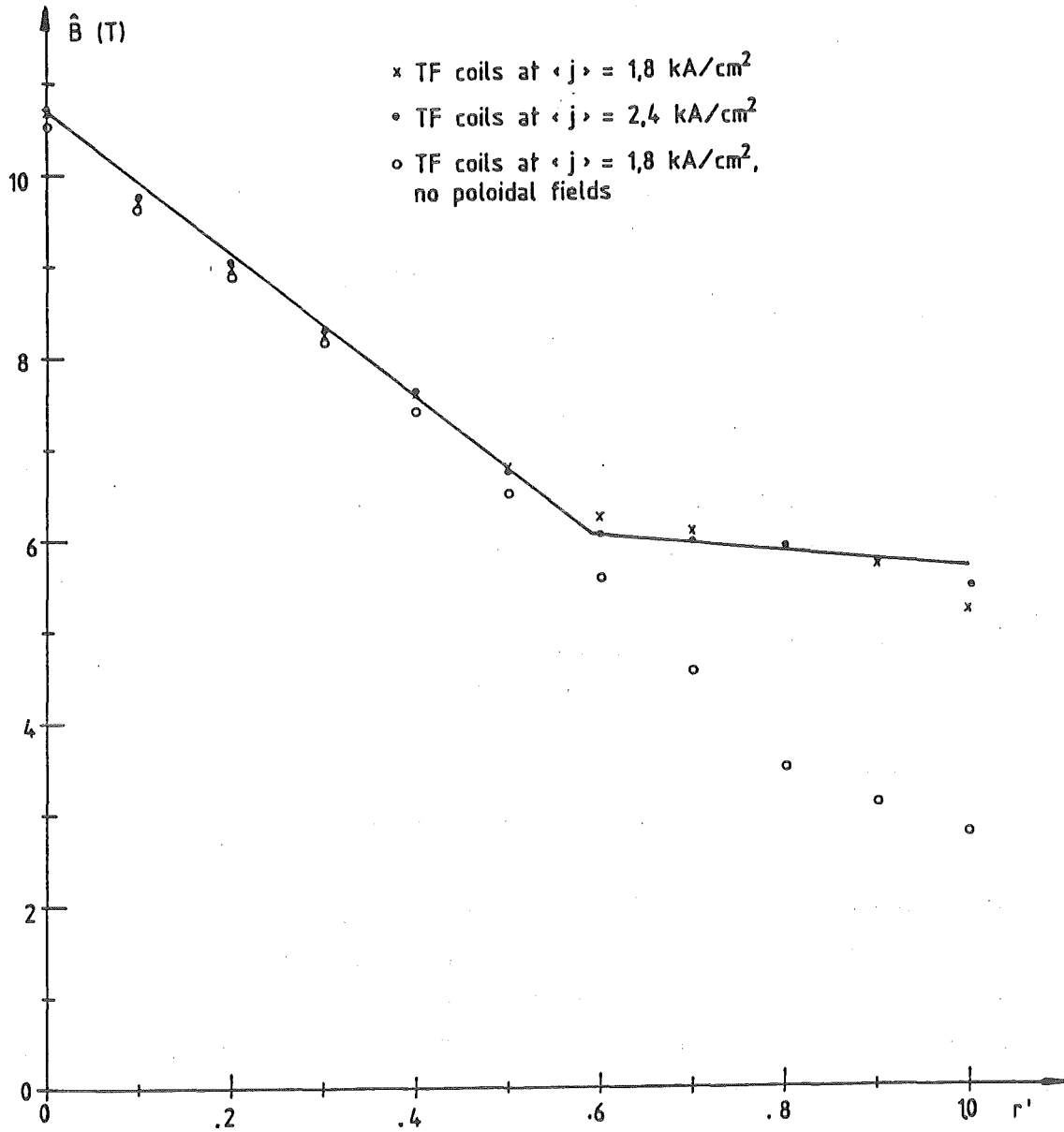
Fig. 3.2-2: Peak field in a TF coil layer vs. the relative radial position of the layer.

3.3 Mechanical Stresses

3.3.1 Bending Stresses

The core is assumed to be wound up and reacted with a minimum radius R_o = 1.5 m. When the core is deformed to a radius R, the strain ε at a distance δ from the neutral bending axis is

$$\varepsilon = \pm \delta (1/R - 1/R_o).$$

Supposing that the neutral axis remains in the core centre, the maximum distance of the Nb_3Sn from the neutral axis is about 2 mm. The maximum strain arises in the straight part of the TF coil $(R = \infty)$:

$$\varepsilon = \pm 2 \text{ mm } (- 1/1.5 \text{ m}) = \mp 0.13\%$$

These strains have to be considered in addition to the strains caused by Lorentz forces during operation.

3.3.2 Mechanical Stresses during Operation

The conductor is mainly subjected to 2 loads:

- the axial tension (hoop forces) and a
- the pressure on the flat side of the conductor.

The value of the hoop forces is about 64 MN per coil, the value of the axial force acting on a single conductor thus being around 160 kN. Due to bending by out-of-plane forces and other effects, however, some conductors may bear a 50 percent higher force (240 kN). For the calculation of the axial conductor strain the following Young's moduli are assumed:

    steel: 210 GPa
    core: 120 GPa
    copper: 120 GPa

The stiffness in winding direction is 106 MN, the overall Young's
modulus of the conductor ~123 GPa.

The mean axial strain becomes ε_m = 160 kN/106 MN = 0.15%,
and the maximum axial strain will be

ε_{max} = ε_m x 1.5 = 0.23%, but not in the straight part of the TF
winding.

The total strain does nowhere exceed the permissible value, about
0.35%, given by the prestrain in bronze-processed Nb_3Sn.

In the straight part of the TF coil the Lorentz forces are taken by
the vault cylinder. The overall maximum pressure on the flat side of
the conductor is subjected to some 55 MPa (see Fig. 3.3-2). The
resulting strain in the Cu-profiles and in the core is nearly the
same as in the short faces of the steel conduit, i.e. $\leq$ 0.06%.
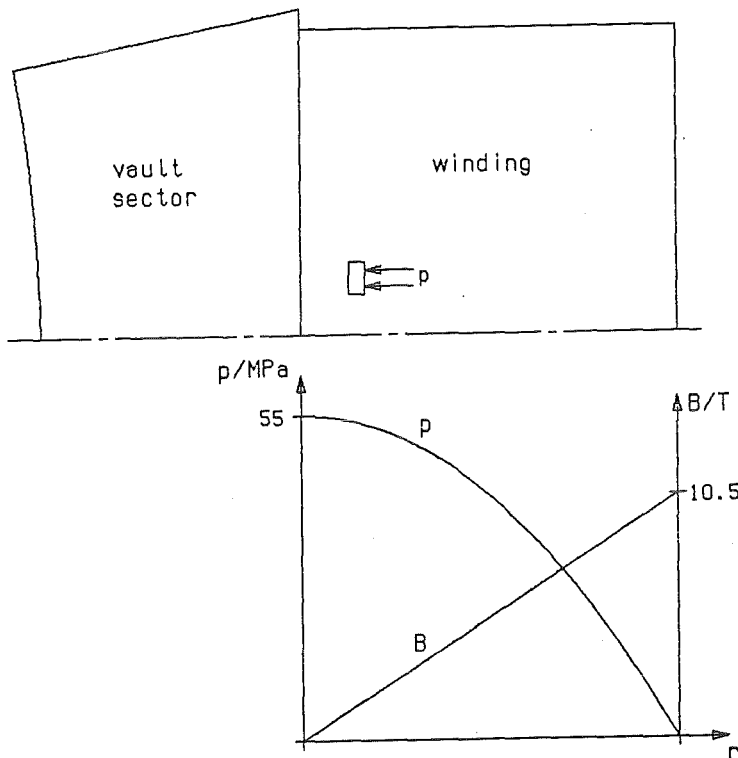
Fig. 3.3-2: Pressure increase in the straight part of a TF winding.

The influence of transverse pressure on the critical current of Nb_3Sn wires is still to be investigated. The pressure enhances the axial strain

by $\Delta \varepsilon_{ax} = \nu \cdot 0.06\% = 0.02\%$ ($\nu = 0.33$: Poisson ratio)

With the radial strain 0.06 % the stress in the steel conduit (short faces) of the conductor becomes 126 MPa. The insulation is also partly loaded with this pressure, but this is not critical, for it can withstand compression stresses exceeding 200 MPa.

3.4 Radiation Effects and Nuclear Heating

3.4.1 General Effects

Superconducting magnets are composed of different materials having a very different behavior under low temperature irradiation conditions. These materials are:

- superconducting materials, e.g. NbTi, Nb_3Sn
- stabilizing materials, e.g. Cu, Al
- structural materials, e.g. stainless steel, solders,
- insulating materials, e.g. GFF epoxies, polyimides,
- coolant He.

In the superconducting materials, irradiation processes change the metallurgical structure by creating defects and/or defect clusters. This has a profound effect on the "overall" properties of interest for the magnet designer. These properties, the transition temperature, T_c, the upper critical magnetic field, B_{c2}, and the electrical resistivity, ρ, have finally a combined effect on the current carrying capacity, J_c.
Irradiation of stabilizing materials considerably changes their resistivity by creating lattice defects and transmutation products. Mechanical properties are also changed but only at high doses. Irradiation of structural materials at doses considered as representative for superconducting magnets seems to have no influence on their properties and will therefore not be considered.

The mechanical and electrical properties of insulating materials are not only affected by neutrons but also by gamma rays. The atomic processes caused by neutron or gamma irradiation are very different, but lead finally to the formation of chemical bonds between chains (cross-linking) and the fracture of the polymer molecule (chain scission). Additional and/or resulting effects are the formation of double bonds (unsaturation), gas evolution by dissociation of small side molecules from the polymer, and reactions with the environment.

The coolant He may be influenced by permeating gases, created in nuclear reactions, e.g. hydrogen, which freezes out and may lead to channel blocking.

A summary of the effects is given in /7/ for superconducting and stabilizing materials. /8/ will describe the behaviour of organics in a neutron and gamma radiation environment.

3.4.2 Conclusions for Superconductors

Some conclusions for the radiation behaviour of NbTi and Nb_3Sn can be drawn as follows.

a) A15 high field superconductors are more sensitive to irradiation than NbTi. The influence of neutron irradiation on T_c and B_{c2} is very small for NbTi. At a dose of 10^{19} n/cm^2 (E > 0.1 MeV), T_c of NbTi is nearly unchanged while T_c for Nb_3Sn is decreased by about 60 %. At a dose of 3×10^{18} n/cm^2 (E > 0.1 MeV) (this fluence is the actual design value), T_c for Nb_3Sn is decreased by about 10%.

b) A fluence of the order of 10^{19} n/cm^2 (fission spectrum) produces only up to 20 % reduction of the critical current of NbTi in fields up to 6 T. The same dose, however, reduces the critical current for Nb_3Sn by about 95 % (specially prepared single core Nb_3Sn specimens were reported to show no degradation at 10^{19} n/cm^2 (E > 0.1 MeV), but single core Nb_3Sn conductors are not relevant for fusion magnets /10/).

c) Irradiation data for Nb_3Sn with additives are not available so far.

It is recommended to assume as design dose for the supercon-
ductors NbTi and Nb_3Sn used in fusion magnets a neutron fluence of
3×10^{18} n/cm^2.

3.4.3 Conclusions for Stabilizing Materials

The low temperature radiation data on the resistivity changes of the
stabilizers Cu and Al show that for a fluence of about 10^{20} n/cm^2
(E > 0.1 MeV) the radiation-induced resistivity in Cu is equal to the
room temperature value. Al reaches that value even for smaller
fluences, e.g. 3×10^{19} n/cm^2 (E > 0.1 MeV). These values cannot be
tolerated, because they would lead to the design of huge magnets.
Therefore a tolerable value must be determined and a periodic warming
up of the magnets must be foreseen to anneal partly or if possible
totally the resistivity induced at low temperatures by radiation. At
room temperature Al anneals completely out, but Cu retains 15 % to
20% of the radiation-induced resistivity. Therefore repeated
annealing experiments with interim exposures to neutron irradiation
at 4.2 K are needed to remove the biggest uncertainty in specifying
the amount of Cu in the cross section of the conductor.

A tolerable value of the resistivity enhancement before the first
anneal seems to be in the order of 20 % to 40 % of the initial
resistivity value. The value eventually chosen is always a design
compromise between operation time (or neutron fluence), amount of Cu
in the cross section of the conductor and number of annealing cycles.

The radiation data reported until now are usually valid for magnetic
fields up to 6 T. The behaviour at high fields and also at high doses
can only be predicted by extrapolation.

For high field applications an assessment of Al and Cu should be made, because the magnetoresistivity of Cu is much higher than that of Al. A general conclusion is that with rising magnetic fields the importance of Al as stabilizing material increases. In the present study, Al was excluded due to its poor mechanical properties.

3.4.4   Conclusions for organic insulators

The neutron and gamma radiation tends to degrade mechanical and electrical properties of organic insulators. Thermosets are ordinarily used as magnet insulation materials filled with glass or carbon fibre fabric (GFF, CFF respectively) as reinforcer. Since the composition is the manufacturer's secret, it is very difficult to get a reliable data base for organics. So, curves for materials properties versus fluence have to be understood as broad bands. Nevertheless, several general conclusions can be drawn:

- organic materials are in general more sensitive to nuclear radiation than other substances, due to their complexity,
- the applicability of the data obtained from small laboratory specimens to large scale devices is uncertain,
- in the radiation regime where organic materials withstand mechanically, the electrical properties practically do not alter,
- materials based on epoxies typically begin to show serious reduction in mechanical properties for doses between 10^6 and 10^7 Gy (10^8 - 10^9 rad), while those based on polyimides show about an order of magnitude improvement (10^7 Gy corresponds to about 10^{18} n/cm^2).

Assuming a 25% decrease in mechanical properties as tolerable at the end of the useful life in a fusion reactor, glass fibre reinforced epoxy can be used at a dose of 2×10^6 Gy (2×10^8 rads) in the case of G-10 CR and at a dose of 3×10^6 Gy (3×10^8 rads) in the case of G-11 CR. The tolerable dose for polyimide based organics is an order of magnitude higher, and therefore to date preference is given to these materials.

3.4.5 Nuclear heating

According to W. Daenner /9/ the absolute value of the peak power density p_{max} is about 0.3 mW/cm^3. The average power density across the inboard coil cross section is thus in the range of 0.043 mW/cm^3 while the corresponding value on the outboard side is lower by a factor of 5. The values are calculated using preliminary data for coil composition (10% superconductor Nb$_3$Sn + Bronze, 30% stainless steel, 30% copper, 20% Helium, and 10% insulation) and using a shield which was not optimized. The curve of Fig. 13 in /9/ for the nuclear heat power density on the inboard side is approximated by an exponential function

$$p = p_{max} \cdot \exp(-x/\lambda) \tag{1}$$

where p_{max} is the peak value on the inboard side, x the actual thickness of the winding measured from the inboard side and λ the decay length.
The result is

$$p = 0.3 \text{ mW/cm}^3 \cdot \exp(-x/9.03 \text{ cm}) \tag{2}$$

For values $x/\lambda \gg 1$,

$$\overline{p} \cdot T = p_{max} \cdot \lambda, \tag{3}$$

where $\overline{p}$ is the average nuclear power density and T the overall radial coil thickness.

The radial coil thickness in /9/ is assumed to be 0.63 m. During the conductor design process the coil geometry was changed leading to a new coil thickness of T = 0.47 m. Using equation (3) and the decay length of λ = 9.03 cm an average power density of 0.058 mW/cm^3 is found. The new coil volume is 8.8 m^3. Therefore the total nuclear heating power in a TF coil is 500 W or 31 W in each of the 16 pancakes. This value is an upper limit because it didn't take into account any decrease along the circumference of the winding from the inboard to the outboard side.

3.4.6 Radiation hot spots

The use of neutral beam injectors with long and broad ducts and/or some vacuum piping causes paths for intense radiation streaming. These "radiation hot spots" may seriously affect the local magnet performance and can drastically change the materials properties in certain winding regions. Therefore careful analysis has to be performed to identify the weakest regions of the radiation shielding for the superconducting fusion magnets.

3.5 AC losses

3.5.1 The NET burn scenario

The NET burn scenario is not yet fully evaluated. For this study, four different stages are considerd: Start up: 15 s; burn phase: 200 s; ramp down: 15 s, and down turn: 15 s. The total cycle time is T = 250 s.

- The loss energy is generated only during the start up and the ramp down time.
- The plasma disruption energy dissipated in the TF coils is not yet considered. It will depend on the blanket and shield time constants.
- Plasma position control needs are not yet defined for NET-II. We therefore want to address a word of warning.

A word of warning

The main difficulty for the cryogenic loss estimation is the still unknown loss contribution in the TF coils due to plasma position control fields. If a considerable induction change rate will be seen by the TF coils, there will be a loss generation during the burn phase too, which could dramatically increase the overall cryogenic losses. If the mean plasma position control field would be 1% of the mean PF coil induction and the control frequency f = 5 Hz, the coupling losses/m would be higher than the losses due to the field rise during the start up phase. The losses could come close to the heat removal capacity of the present conductor design.

For the present NET-II design, mean PF coil induction values transverse to the TF coil perimeter $\overline{B}_n$ and parallel to the TF coil perimeter $\overline{B}_t$ are given in Table 3.5-1.

	$|\overline{B}_n|(T)$	$\overline{B}_n^2 \, (T^2)$	$\overline{B}_t \, (T)$	$\overline{B}_t^2 (T^2)$
outside	0,82	1,06	0,8	1,17
middle	0,63	0,6	0,68	0,77
inside	0,49	0,38	0,63	0,58

Table 3.5-1: Mean values of the PF coil induction

Due to the field dependence of the stabilizer resistivity and the dependence of the induction on the TF coil circumference, coupling and hysteresis losses locally may be increased by a factor of 10 compared to the average value.

3.5.2 Hysteresis losses

The hysteresis losses have been calculated considering the local variation of critical current, PF coil induction and the ratio of critical current to transport current.

The mean loss energy is

$$q = 62 \text{ mJ per meter.}$$

These losses can be neglected in this study.

3.5.3 Coupling losses due to the transverse PF coil induction

The eddy current losses in a complex conductor configuration as shown above can only be calculated by some simplifications. The conductor consists of several components having different geometric arrangements and just so different electrical properties. Thus the conductor is in reality an electromagnetically and galvanically coupled system of inductive loops. For a first estimation of losses the attempt will be made to treat the problem by a simple formula and a convenient averaging of the different electrical properties. The released eddy current energy in a homogeneous system, penetrated by the linear increase or decrease of the transverse field ΔB, can be described in general by the following expression /21/

$$E = \frac{(\Delta B)^2}{\mu_0} \frac{\tau}{T} V \qquad [\text{Joule}]$$

Herein means the time constant of the system, T the time period of field change with $T \gg$, and V the volume occupied by the system, e.g. the conductor. Since the conductor has mainly a rectangular geometry the time constant of a slab geometry is a very appropriate approximation

$$\tau = \frac{\mu_0 \ell_0^2}{\varrho \pi^2}$$

l_c is a characteristic length, in twisted superconductors half of the twist pitch l_p respectively the transposition length in a cable, and ϱ is the resistivity. Thus in a complex conductor configuration the task is shifted to find a good approximation for the average resistivity.

The inductive electromagnetic voltage forces screening currents in general parallel to the axis of the conductor having components in the normal conducting matrix (mainly perpendicular to the conductor axis) and in the superconducting paths. A general simplified flow pattern of the screening currents through the normal conducting matrix is given in Fig. 3.5-1. On the basis of this pattern and the geometric sizes of the whole conductor arrangement the individual resistances were calculated. The resistivity values of the different components used here for the calculation are

$$\rho_{Cu} = 4 \cdot 10^{-10} \ \Omega\,m \ \text{(at 6 T)}$$

$$\rho_{bronze} = 3.2 \cdot 10^{-8} \ \Omega\,m$$

$$\rho_{solder} = 1.6 \cdot 10^{-8} \ \Omega\,m$$

$$\rho_{CuNi} = 1.4 \cdot 10^{-7} \ \Omega\,m$$

$$\rho_{sc} = \rho_{bronze} \cdot \frac{1-\lambda}{1+\lambda} = 1.96 \cdot 10^{-8} \ \Omega\,m \ (\lambda = 0.24).$$
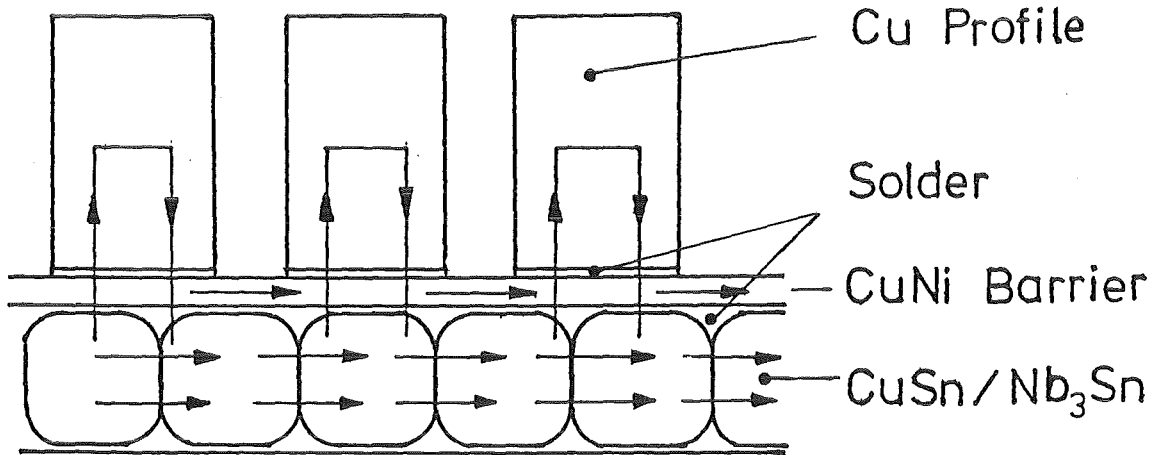
Fig. 3.5-1: The expected flow pattern of the screening currents in the
NET-II conductor

The total resistance for all the parallel currents was then evaluated
and finally expressed in terms of resistivity for the overall conduc-
tor cross section excluding the steel case. This results in a resi-
stivity value of

$$\langle \rho \rangle = 4.33 \cdot 10^{-8} \ \Omega\,m$$

leading to a time constant of

$$\tau = 81 \ \text{ms}.$$

assuming a transposition length of 33 cm. These fundamental mean
electric properties of the cable and the characteristic data of the

magnetic field varying linearly in time, $((< B^2 >)^{1/2} = 0.82 \; T_r$ and $T_r = 15$ s) lead to losses for the increasing field of

$$\frac{P}{L} = \frac{\Delta B^2}{\mu_0} \cdot \frac{\tau}{T_r^2} V \qquad = 98 \; m \; W \; per \; meter$$

The losses in a pancake containing 650 m of conductor amounts to

$$P_p = 63.8 \; Watt$$

Regarding the full trapezoidal field cycle and the repetition rate the mean eddy current losses for the transversal field component are

$$P = 7.7 \; Watt$$

A loss contribution from the superconducting strands and the stabilizing copper profiles can be neglected because the time constants are small in the range of 10^{-3} s, respectively $2.6 \cdot 10^{-3}$ s leading to losses nearly two orders of magnitude smaller than for the cable. The importance of the CuNi resistive barrier for reducing the eddy current losses can be seen from the average resistivity without a barrier

$$< \rho > = 1.1 \cdot 10^{-8} \; \Omega \, m$$

That value would lead to more than three times higher losses.

3.5.4 The necessity of the folded insulating strip

In order to give an impression of the necessity of the core insulation, the losses are calculated, assuming a hypothetical CuNi strip of 0.5 mm thickness, which is not insulated. The losses are given by

$$\frac{P_c}{L} = \frac{\dot{B}^2}{T_r^2} \cdot \frac{(2H)^2}{\rho C} \cdot \frac{\ell_p^2}{120} \, (2H)$$

where 2H is the width and C is the thickness of the core. The effective conductivity $\frac{(2H)^2}{C} \cdot \frac{1}{\rho}$ is calculated taking the geometry of Fig. 2.2-3:

$$\frac{(2H)^2}{\rho C} = 1.86 \cdot 10^7 \; \Omega^{-1}$$

The losses per unit length would result as $P_c/L = 2,58$ W/m. A reliable insulation of the core is therefore mandatory.

3.5.5 Losses due to the tangential poloidal induction

The TF coil is exposed to large tangential induction change rates. The superconducting cable and the stabilizer both are long solenoids with turn numbers of $L/l_p = 650$ m/0.33 m = 1625 and 650/1 = 650 respectively. The tangential induction change rate induces voltages between the turns of the windings which cause transverse currents through the matrix and thus losses. The geometry is taken from Fig. 2.2-2. The effective area which is exposed to the changing field is considered as $A = (5.1+3.6) \times 37$ mm and the length of the current path as $l = 2 \times (5,1+3,6+37)$ mm. The effective conductivity of the matrix results to δ/ρ 4.95 . $10^4 \Omega^{-1}$ where $\delta = 8.7$ mm and ρ taken from 3.5-3.

The mean value of this induction change rate is $\overline{B}_t^2 = 0.84$ T^2. The losses are given by

$$ P_t/L = \frac{\overline{B}_t^2}{T_r^2} \cdot \frac{A^2}{\ell} \cdot \frac{\delta}{\rho} $$

and result as $P_t/L = 0,21$ mW/m, which is negligible.

The tangential induction change does not cause net superconducting currents flowing through the power supply, because the net flux swing with respect to the power supply is zero in the tokamak configuration.

3.5.6 Resistive barrier and electrical stability

It is to be expected that the resistive barrier between the superconductor and the stabilizer will not impair the electrical stability. A few experiments with resistive barriers have given no indication for a reduction of electrical stability /29/. The resistive barrier enhances the transfer length of the current transition from the normal conducting superconductor into the copper stabilizer, as given by

$$ \ell_o = \sqrt{\frac{\rho_\perp}{\rho_\parallel}} \sqrt{dc} \qquad [cm] $$

where $\rho_{\perp}$ is the resistivity of the CuNi barrier and $\rho_{\parallel}$ that of the bronze matrix and d is the diameter of the superconducting strands and c the thickness of the barrier. The transfer length in the cable is about 2 mm. Because of the transient existence of a normal conducting zone the heat production in the transfer region and the heat flux density along the conductor will be a reasonable measure for a comparison with experimental results. This heat flux density is given by

$$q_{tr} = \rho_{bronze} \cdot j_o^2 \cdot l_o$$

It amounts in the NET-II conductor to

$$q_{tr} = 443 \ W/cm^2 .$$

In an experiment with a resistive layer of brass (0.25 mm thick), a transfer length of 0.42 mm was evaluated. Up to a heat flow rate of $q_{tr} = 467 \ W/cm^2$ no influence on the recovery behaviour was observed in that conductor /29/. The expected heat flux density and the experimental one are nearly the same so that the recovery in the NET-II conductor should not be impaired by the resistive barrier.

3.5.7 Summary of the loss calculations

The loss calculations have been carried out without considering plasma position control losses. These losses might completely change the picture. For this study we can neglect the hysteresis losses.

The coupling losses in one hydraulic channel during one pulse of T = 250 s yield:

$$P_p = 650 \ m \cdot 98 \ mW/m \cdot 30/250 \cdot 3 = 23 \ W$$

The factor 3 reflects the differences between measurements and calculations for the Euratom LCT conductor /3/.

The total coupling losses in all 16 TF pancakes are thus 368 W.

3.6 Cryogenic layout

The internal coolant flow has to meet two requirements:

- removal of the total heat load,
- stabilization of the superconductor.

This must be done under the constraints of

. tolerable cross section area of the winding,
. acceptable friction losses.

The optimization of such a system would imply the variation of many parameters, not only of the fluid parameters such as flow rate and operational conditions, but also the variation of the total set-up of the conductor, mainly the layout of the cryostabilizing region. A consequent optimization of such a system might be possible by iterative heuristic processes only.

Helium flow in a heated channel

Pressure and temperature in a heated flow of a compressible fluid are given by /11/

$$\frac{dp}{dz} = \frac{\dfrac{2fG^2}{\rho D} + \dfrac{4qG\beta}{\rho D(C_p - v^2\beta)}}{1 - \dfrac{G^2}{\rho}(K + \beta\varphi)} \tag{1}$$

and

$$\frac{dT}{dz} = \frac{\dfrac{4q}{GD(C_p - v^2\beta)} - \dfrac{2fG^2\varphi}{\rho D}}{1 - \dfrac{G^2}{\rho}(K + \beta\varphi)} \tag{2}$$

with

$$\varphi = \frac{-\left(\dfrac{\partial H}{\partial p}\right)_T + v^2 K}{C_p - v^2\beta}$$

The used symbols are:

Z   length coordinate (m),

p   pressure (Pa),

f   friction factor,

G   mass flow velocity $(kg/(m^2.s)$

      density of the bulk fluid (kg/m^3),

D   hydraulic diameter,

ß   coefficient of expansion,

K   compressibility

q   heat flux from the wall to the fluid (W/m^2),

C_p specific heat $(J/kg .K)$

v   flow velocity (m/s),

H   specific enthalpy (J/kg)

The coolant channel under consideration is a system of many equally sized rectangular ducts. The overall hydraulic diameter is by definition

$$D = \frac{4 A_{He}}{P_{He}} \tag{3}$$

where A_{He} is the helium flow area, P_{he} is the wetted perimeter, and the mass flux is

$$G = \frac{\dot{m}}{A_{He}} = \rho v \tag{4}$$

The permanent heat load is

$$q = \frac{dQ}{dz} \cdot \frac{\lambda}{P_{He}}$$

(5)

where dQ/dz is the heat load per unit length (see 3.7.4).

The configuration of the present coolant channels is similar to that of the Euratom-LCT conductor (helical ducts with many interconnections)). Measurements on the LCT conductor show that the friction factor is approximately twice the value of a smooth tube /12/ which is given by Arp et al. /1/,

$$f_o = 0.046 \cdot Re^{-0.2} \cdot$$

(6)

In the NET-II conductor design,

$$f = 2 \cdot f_o$$

(7)

is used. The helium state equation

$$\rho = \rho(p, T)$$

(8)

as well as the transport quantities such as viscosity and thermal conductivity are given by computer codes /13,14/.

Herewith, the numeric integration of (1) and (2) yields temperature

$$T = T(Z, \dot{m}, T_i, p_i, D, dQ/dz)$$

(9)

and pressure

$$p = p(Z, \dot{m}, T_i, p_i, D, dQ/dz)$$

(10)

of the fluid. Other quantities of interest such as Re, Pr and the flow velocity are also computed.

Forced flow heat transfer

For safe operation of the magnet the temperature of the bulk fluid, T_b, must have a sufficient margin, ΔT, from the critical temperature, T_c, of the superconductor. This safety margin, ΔT, depends on the philosophy of stabilization and of protection of the coil. A conservative design may be based on the Stekly criterion

$$\alpha_{st} = \frac{I^2 \cdot S_{Cu}}{A_{Cu} \, \rho_{Cu} \, h \, (T_c - T_F)} \leq 1 \qquad (11)$$

The upper limit with $T_c = T_w$ (T_w = surface temperature of the stabilizing copper) and $\alpha_{st} = 1$ is used in the calculation.

The heat transfer coefficient, h, is a complex function of flow velocity, coolant channel geometry, helium state and heat flux. For small heat fluxes to single phase forced flow it may be calculated from the Dittus-Boelter correlation

$$Nu_{DB} = 0.023 \cdot Re^{0.8} \cdot Pr^{0.4}$$

and from the definition of the Nusselt number

$$Nu = hD/\lambda \qquad (13)$$

when λ is the thermal conductivity of the bulk helium.

Measurements of heat transfer of supercritical helium at forced flow, however, show deviations from formula (12) to both higher and lower values /15,16/. Both effects are described by the empirical formula of Giarratano /5/, i.e.

$$Nu_G = 0.0256 \cdot Re^{0.8} \, Pr^{0.4} \, (T_w/T_b)^{-0.716} \qquad (14)$$

More recent investigations /17,18,19/ show that this formula predicts too high values close to the transposed critical line. Therefore, the

more recent correlation of Yeroshenko and Yaskin /6/ with

$$Nu_{yy} = 0.023 \, Re^{0.8} \, Pr_b^{0.4} \left(\frac{2}{\sqrt{0.8\psi + 0.2} + 1} \right)^2 \cdot F \tag{13}$$

is used, where

$$\psi = 1 + \beta_b \, (T_W - T_b) \tag{14}$$

and

$$F = \begin{cases} (\bar{c}/c_{p,b})^{0.28} & , \text{ for } \bar{c}/c_{p,b} > 1 \\ \\ 1 & , \text{ for } \bar{c}/c_{p,b} < 1 \end{cases} \tag{15}$$

$\bar{c}$ describes the mean specific heat of the laminar boundary layer

$$\bar{c} = \frac{H_w - H_b}{T_W - T_b} \tag{16}$$

This formalism has also been implemented into the computer code and it calculates the local temperature, T_w, of the copper surface for the Stekly condition (11). (The local resistivity of copper is given in 3.7.)

In Fig. 3.6-1 the ratio of this Nusselt number to that of the Dittus-Boelter correlation is plotted vs. the quantity ψ. The dashed curves at $1 < \psi \leq 3$ describe only qualitatively the enhancement effect which becomes the more pronounced the more the critical point of the helium is approached. More accurate quantitative data are given in Tab. 3.6-1, rows 12 and 16.
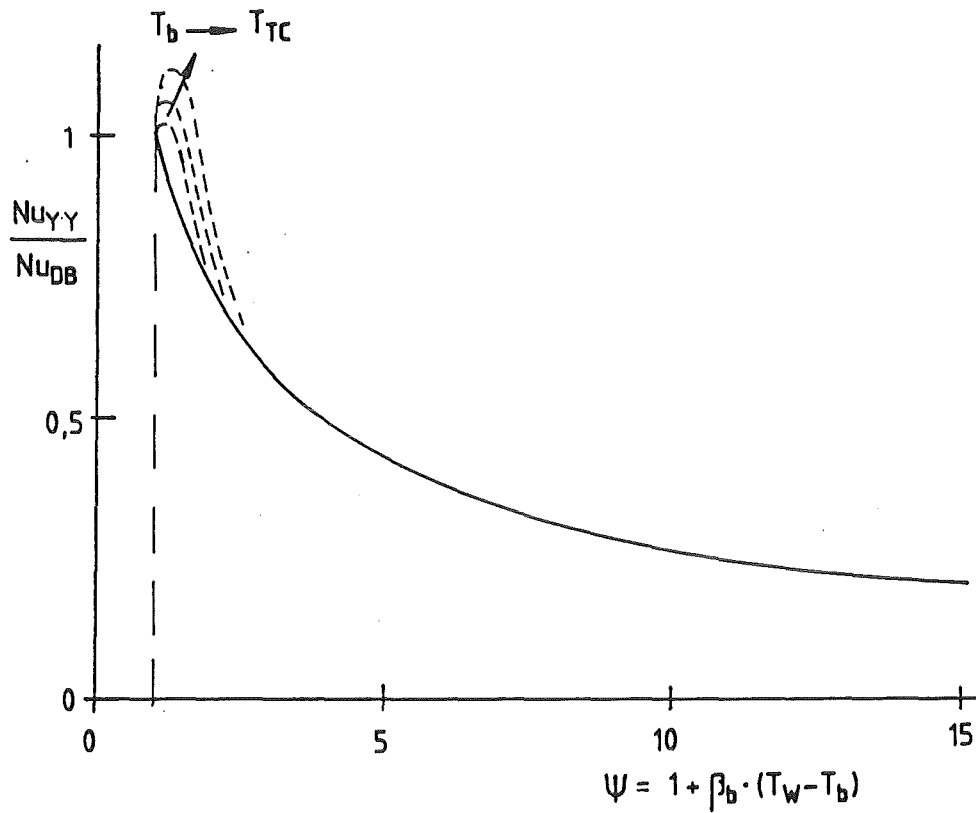
Fig. 3.6-1: Correlation for turbulent heat transfer to supercritical helium /16/.

Numerics

The numeric analysis is based on the corresponding program HEHT (Version 1974) of V. Arp (NBS) which uses a modified Runge-Kutta procedure to integrate the differential equations in a duct with circular cross section. This program has been modified for the hydraulic cross section of the present conductor design. Further, the NBS helium subroutines /13/ have been replaced by the recently updated Oxford subroutines /14/. Those subroutines are written in SI Units. Thus it becomes more comfortable to modify the main program.

Table 3.6-1: Input and output list of the thermodynamical computation.
Symbols are explained in the text.

```
C   MUSTER FUER EINGABE ZU  $HEH2   MIT DATEI2
C
C   EINGABE FUER : NET-ENTWURF      DATUM:  6.11.1984
C
C   DELI IS THE INITIAL INTEGRATION STEP: =DELZ/2**N ; N=Ø OR POSIT.
C
C   L=65Ø-X
C   FQOHM=ST*ST/ACU/PHE*(3.85+2.15*(364-X)/364)*E-1Ø
C   FUER X GROESSER 364 M
C   FQOHM=CONST  SONST
C
C   ADQDZ=.Ø33+.Ø36*(65Ø-Z)/65Ø+.26*EXP((-(65Ø-Z)/12Ø) IN W/M
C   PATMI,TI,   ZMF,DELZ,DELI, ACRCY,   GS,   DIAM,   AFLOW,
C   (BAR) (K)   (M)  (M)  (M)          (G/S)  (CM)    (CM**2)
1 **   6.   4.7 65Ø.  25.  25.   .ØØ5   5.    .157    .936
C   SAR   DQDZ,     JDF,JQF,JTSTAG,JDELT AMP  ACU  JDIR
C   (CM)  (W/M)                          (A)  (MM2)
2 **   21.3  .1       Ø   1    Ø     1    1984Ø 229   1
```

Z METER	DIAM CM	DQ/DZ WATT/M	P ATMOS	T KELVIN	RHO GM/CM3	FFRIC	VELOC. M/S	RE NUMBER	H W/(CM*K)	DEL T KELVIN	NU/NUØ	TW K	QOHM W/CM2	/	IFAIL	PSI
Ø.Ø	Ø.176	Ø.293	6.ØØØ	4.7Ø6	Ø.13734	Ø.Ø12	3.9D-Ø1	22831.	Ø.ØØ87	5.4Ø1	1.Ø1Ø	1Ø.1Ø7	Ø.484		Ø	1.545
25.ØØ	Ø.176	Ø.245	5.917	5.Ø72	Ø.1312Ø	Ø.Ø12	4.1D-Ø1	24Ø78.	Ø.Ø97Ø	5.176	Ø.94Ø	1Ø.248	Ø.472		Ø	1.659
5Ø.ØØ	Ø.176	Ø.2Ø7	5.831	5.331	Ø.126Ø1	Ø.Ø12	4.2D-Ø1	25147.	Ø.1Ø26	5.Ø16	Ø.893	1Ø.347	Ø.46Ø		Ø	1.757
75.ØØ	Ø.176	Ø.176	5.742	5.528	Ø.12157	Ø.Ø12	4.4D-Ø1	26Ø58.	Ø.1Ø81	4.9Ø1	Ø.846	1Ø.429	Ø.448		Ø	1.869
1ØØ.ØØ	Ø.176	Ø.152	5.651	5.679	Ø.11758	Ø.Ø12	4.5D-Ø1	26898.	Ø.1132	4.8Ø9	Ø.8Ø1	1Ø.488	Ø.437		Ø	1.987
125.ØØ	Ø.176	Ø.132	5.557	5.796	Ø.11396	Ø.Ø12	4.7D-Ø1	276Ø8.	Ø.1181	4.732	Ø.759	1Ø.528	Ø.425		Ø	2.111
15Ø.ØØ	Ø.176	Ø.116	5.461	5.887	Ø.11Ø63	Ø.Ø12	4.8D-Ø1	28415.	Ø.1227	4.667	Ø.72Ø	1Ø.553	Ø.413		Ø	2.241
175.ØØ	Ø.176	Ø.1Ø3	5.363	5.957	Ø.1Ø754	Ø.Ø12	5.ØD-Ø1	29117.	Ø.1272	4.61Ø	Ø.683	1Ø.567	Ø.4Ø1		Ø	2.378
2ØØ.ØØ	Ø.176	Ø.Ø93	5.262	6.Ø13	Ø.1Ø463	Ø.Ø12	5.1D-Ø1	29796.	Ø.1315	4.559	Ø.647	1Ø.571	Ø.389		Ø	2.525
225.ØØ	Ø.176	Ø.Ø85	5.159	6.Ø55	Ø.1Ø184	Ø.Ø12	5.2D-Ø1	3Ø461.	Ø.1358	4.398	Ø.63Ø	1Ø.453	Ø.377		Ø	2.635
25Ø.ØØ	Ø.176	Ø.Ø79	5.Ø54	6.Ø88	Ø.Ø9915	Ø.Ø12	5.4D-Ø1	3112Ø.	Ø.14Ø1	4.219	Ø.617	1Ø.3Ø7	Ø.365		Ø	2.739
275.ØØ	Ø.176	Ø.Ø75	4.946	6.111	Ø.Ø9651	Ø.Ø12	5.5D-Ø1	31782.	Ø.1443	4.Ø45	Ø.6Ø4	1Ø.156	Ø.353		Ø	2.844
3ØØ.ØØ	Ø.176	Ø.Ø71	4.836	6.127	Ø.Ø9391	Ø.Ø12	5.7D-Ø1	32452.	Ø.1486	3.874	Ø.592	1Ø.ØØ1	Ø.341		Ø	2.945
325.ØØ	Ø.176	Ø.Ø68	4.723	6.136	Ø.Ø9131	Ø.Ø11	5.9D-Ø1	33139.	Ø.153Ø	3.7Ø7	Ø.58Ø	9.843	Ø.329		Ø	3.Ø55
35Ø.ØØ	Ø.176	Ø.Ø66	4.6Ø7	6.14Ø	Ø.Ø8869	Ø.Ø11	6.ØD-Ø1	33846.	Ø.1574	3.54Ø	Ø.569	9.68Ø	Ø.317		Ø	3.159
375.ØØ	Ø.176	Ø.Ø65	4.489	6.138	Ø.Ø86Ø4	Ø.Ø11	6.2D-Ø1	3458Ø.	Ø.1618	3.472	Ø.552	9.611	Ø.311		Ø	3.325
4ØØ.ØØ	Ø.176	Ø.Ø64	4.367	6.131	Ø.Ø8335	Ø.Ø11	6.4D-Ø1	35347.	Ø.1663	3.54Ø	Ø.527	9.67Ø	Ø.311		Ø	3.596
425.ØØ	Ø.176	Ø.Ø64	4.241	6.118	Ø.Ø8Ø59	Ø.Ø11	6.6D-Ø1	36153.	Ø.17Ø7	3.621	Ø.5Ø2	9.738	Ø.311		Ø	3.9ØØ
45Ø.ØØ	Ø.176	Ø.Ø64	4.112	6.Ø99	Ø.Ø7777	Ø.Ø11	6.9D-Ø1	37ØØ2.	Ø.1749	3.716	Ø.477	9.815	Ø.311		Ø	4.237
475.ØØ	Ø.176	Ø.Ø64	3.979	6.Ø75	Ø.Ø7486	Ø.Ø11	7.1D-Ø1	379Ø3.	Ø.179Ø	3.826	Ø.453	9.9Ø1	Ø.311		Ø	4.6Ø7
5ØØ.ØØ	Ø.176	Ø.Ø65	3.841	6.Ø45	Ø.Ø7186	Ø.Ø11	7.4D-Ø1	38863.	Ø.1829	3.946	Ø.43Ø	9.991	Ø.311		Ø	4.996
525.ØØ	Ø.176	Ø.Ø65	3.698	6.ØØ9	Ø.Ø6878	Ø.Ø11	7.8D-Ø1	39884.	Ø.1863	4.Ø79	Ø.4Ø8	1Ø.Ø88	Ø.311		Ø	5.42Ø
55Ø.ØØ	Ø.176	Ø.Ø66	3.548	5.966	Ø.Ø6564	Ø.Ø11	8.1D-Ø1	4Ø97Ø.	Ø.1893	4.238	Ø.387	1Ø.2Ø3	Ø.311		Ø	5.88Ø
575.ØØ	Ø.176	Ø.Ø67	3.393	5.914	Ø.Ø6238	Ø.Ø11	8.6D-Ø1	42152.	Ø.1923	4.426	Ø.365	1Ø.341	Ø.311		Ø	6.433
6ØØ.ØØ	Ø.176	Ø.Ø68	3.229	5.853	Ø.Ø5897	Ø.Ø11	9.1D-Ø1	43456.	Ø.1949	4.651	Ø.342	1Ø.5Ø4	Ø.311		Ø	7.Ø6Ø
625.ØØ	Ø.176	Ø.Ø69	3.Ø57	5.78Ø	Ø.Ø5538	Ø.Ø11	9.6D-Ø1	44911.	Ø.197Ø	4.9Ø8	Ø.321	1Ø.688	Ø.311		Ø	7.75Ø
65Ø.ØØ	Ø.176	Ø.Ø7Ø	2.874	5.695	Ø.Ø516Ø	Ø.Ø11	1.ØD+ØØ	46561.	Ø.1977	5.179	Ø.3Ø3	1Ø.874	Ø.311		Ø	8.415

Finally, the mentioned heat transfer correlations have been implemented with a new subroutine to evaluate the surface temperature.

An example of a numerical run is shown in Tab. 3.6-1. The inputs data are: inlet pressure and temperature (PATMI, TI), total hydraulic length (ZMF), flow rate (GS), helium area (AFLOW), wetted perimeter (SAR), total current (AMP) and copper area (ACU). The quantity JDIR describes the direction of the flow (- 1 for inlet at low field and + 1 at high field). The output list contains both, the parameters of the bulk fluid (P,T,RHO,...RE,H (Dittus-Boelter heat transfer coefficient)), and the data of the thermal boundary layer (DELT = TW-T, TW, Nu/Nu$_o$ and PSI which are caused by the local Ohmic losses, QOHM, in the stabilizer.

The surface temperature TW is one limiting quantity (TW < T$_c$). The other is the friction loss which requires the work

$$W_f \approx \frac{\dot{m} \, \Delta p}{S} = GS \, (P(0) - P(L)).$$

This quantity should be much smaller than the steady heat load (Q DQ/DZ . L).

3.7   Overall design

3.7.1   Ground rules

In addition to the numerical data for superconductor properties, environmental conditions and thermohydraulics of liquid helium presented in Sections 3.1 to 3.6, the following ground rules are set for conductor optimization:

- Cabled core of Nb$_3$Sn strands surrounded by a highly resistive conduit (e.g. CuNi) to reduce ac losses, a cryostabilizing region of Cu profiles and forced flow supercritical helium, and a steel conduit with outside insulation to carry the bulk mechanical loads. The material composition of the conductor is not graded.

- Winding the conductor into a number of identical pancakes. They are assembled into a coil of rectangular cross section in agreement with the spatial constraints of NET-II. The centering forces are carried by a central vault situated radially inward of the TF coils.

- Pancakes are operated in parallel for the LHe-circuit. The channel length is given by the conductor length of a pancake. Flow losses occurring in a pancake ($P_{flow} = \dot{m}\,\Delta p/\rho$) are kept below 25 % of losses due to nuclear heating, ac losses, and heat conduction and radiation from outside. This leaves a reasonable margin for pumping efficiency and heat exchanger design.

- In normal operation, the helium temperature must remain below the "current sharing temperature", $T_s(B,I)$, which is the critical temperature of the superconductor at the local field and at full operating current.

- The conductor should be fully stabilized against "local" disturbances: the temperature of the metal surfaces which are directly cooled by helium must not exceed the critical temperature of the superconductor, $T_c(B,I = o)$, even if the full operating current is carried by the stabilizing copper. This means $\alpha = 1$ for the Stekly criterion. The disturbance is considered "local" and "transient" as long as its total heat input does not change the bulk properties of the helium. This assumption can be justified based on the operational experience of the Euratom/ LCT coil and on the fact that even at low temperatures the heat capacity of metals becomes significant at sufficiently high temperature differences tolerable in a Nb_3Sn coil (for instance, the heat capacity of steel is 130 mJ/cm^3 between 5.5 K and 10 K).

- The average current density should be optimized.

3.7.2 Number of Pancakes and Windings

With a total coil current of about 8 MA and an operational current of about 20 kA, the total number of windings is about 400. They can be provided in i pancakes of j turns each, giving a total coil width $W = i \cdot w_c$ and radial thickness $T = j \cdot h_c$, where w_c and h_c are the width and height of a conductor. The NET-II geometry imposes a 16 coil TF-system and a radial position of 2.495 m for the inner surface

of the straight legs of the TF coils. Thus, for rectangular winding, the condition holds that

$$W \leq \frac{\pi}{8}(2,495 \text{ m} - T) - 0.03 \text{ m}$$

with 0.03 m taken as the minimum distance required between the winding packs of two adjacent coils.

As it seems advantageous to have T as small as possible (small cooling channel lengths, more space for vault), the numbers of pancakes and windings are determined by the conductor dimensions only. An example: w_c = 5 cm, h_c = 2 cm implies 14 pancakes of 28 turns each.

3.7.3 Conductor dimensions

The considerations for determining the conductor dimensions start out by looking at the core. The basic strand dimension of 1.92 mm $\emptyset$ is an upper limit for avoiding a degradation of critical current density due to bending strains. Together with the folded insulating strip of 0.5 mm, soldering material of 1/10 mm and a CuNi conduit around the Nb_3Sn cable, a core height h_c = 5.1 mm results. The width of the core, w_c, depends on the actual critical current and possibly on the stabilizing and reinforcing problem. With a Cu content of 23% in the Nb_3Sn strands, the average volume fraction of copper in the core amounts to

$$\eta_{Cu,core} = 12.7\%,$$

The number and dimensions of the stabilizing copper strands, roebled around the core, can be approached with arguments of cooling and fabrication:

- The roebling process of the copper profiles depends on their aspect ratio A (height/width). Industrial experience favors A = 1.6, in particular for avoiding contacts between adjacent profiles at the Roebel transitions.

- Helium cooling must provide sufficient mass flow in order to keep the bulk helium temperature below the current sharing temperature T_s, and it must also provide sufficient mass flow density (or helium flow velocity) to achieve a large heat transfer coefficient

between metal surface and bulk fluid. This means that the total
helium channel cross section should be kept as small as possible to
increase the mass flow density at a given total mass flow.
Fabrication arguments dictate a lower limit for the width of the
helium channels, w_{He} $\left(w_{He} = 1.0 \text{ mm is chosen}\right)$.

To summarize, for further considerations the following parameters are
fixed:

Core height $\qquad\qquad\qquad\qquad\qquad\qquad\quad$ h_{core} $\quad$ = 5.1 mm,

Copper content in core (volume fraction) $\eta_{Cu, core}$ = 12.7%,

Aspect ratio of copper profiles $\qquad\qquad\qquad$ A $\qquad$ = 1.6,

Width of helium channels $\qquad\qquad\qquad\quad$ w_{He} $\qquad$ = 1 mm.

The purpose of the Copper profiles is to provide stability during a
local normal excursion which is governed by the Stekly equation

$$p_{met} \cdot A_{Cu} = I^2/(\sigma q) \qquad \text{with}$$

p_{met} : cooled perimeter of conductor,

I : operational current,

$\sigma = \sigma(B)$: conductivity of copper,

q: permissible heat flux density into helium.

Using N for the number of copper profiles to be used, very simple
geometric arguments give:

$$A_{Cu} = N \cdot A \cdot w_{Cu}^2 + \eta_{Cu, core} \cdot h_{core} \cdot w_{core}, \qquad (1)$$

$$p_{metal} = N \cdot (2Aw_{Cu} + w_{He}), \qquad (2)$$

$$(h_{core} + 2Aw_{Cu}) \times (w_{core} + 2w_{Cu}) - w_{core} \cdot h_{core} \qquad (3)$$

$$= N \cdot Aw_{Cu}(w_{Cu} + w_{He})$$

These equations can be combined to give a form

$$f(w_{Cu}) \cdot N^2 - g(w_{Cu}) \cdot N = I^2/(\sigma q) \qquad (4)$$

which allows the calculation of widths and heights for different q
and w_{Cu}, in particular the calculation of w_{core}.

The final step is now a determination of the thickness t_{st} of the steel conduit the inner perimeter of which is given by

$$p_{St} = 2.(w_{core} + 2 w_{Cu} + h_{core} + 2 Aw_{Cu}). \qquad (5)$$

With a vault being used to take the centering forces, we assume that each conductor has to carry the average hoop forces of 160 kN in the densely packed winding at a tolerable strain $\mathcal{E}$ of 0.2%. For a rough first layout only the core area at a Young's modulus E_{core} of 120 GPa and the steel area at a Young's modulus E_{St} of 210 GPa are used to contribute to the strength because the highly conducting copper will be subjected to radial pressure by the build up of the centering forces:

$$160 \text{ kN} = \mathcal{E}(w_{core} . h_{core} . E_{core} + p_{St} . t_{St} . E_{St}) \qquad (6)$$

from which t_{st} is derived. Adding 0.5 mm thick insulation around the steel conduit, we now get

$$w_c = w_{core} + 2 w_{Cu} + 2 t_{St} + 1 \text{ mm, and}$$

$$\qquad (7)$$

$$h_c = h_{core} + 2Aw_{Cu} + 2 t_{St} + 1 \text{ mm.}$$

Fig. 3.7-1 shows the relevant dimensions in dependence on w_{Cu} for heat flux densities of .3 W/cm^2, .4 W/cm^2, and .5 W/cm^2 into the helium. It should be mentioned that the product $h_c . w_c$ and therefore also the average current density is essentially independent of w_{Cu}. It is hence possible to choose the conductor with the least width permitted by the critical current limit in the core giving the advantages of least ac losses and a minimum length for the helium channels. The procedure described can be maintained when certain constraints such as strain, core height, or aspect ratio of the copper profiles are altered.
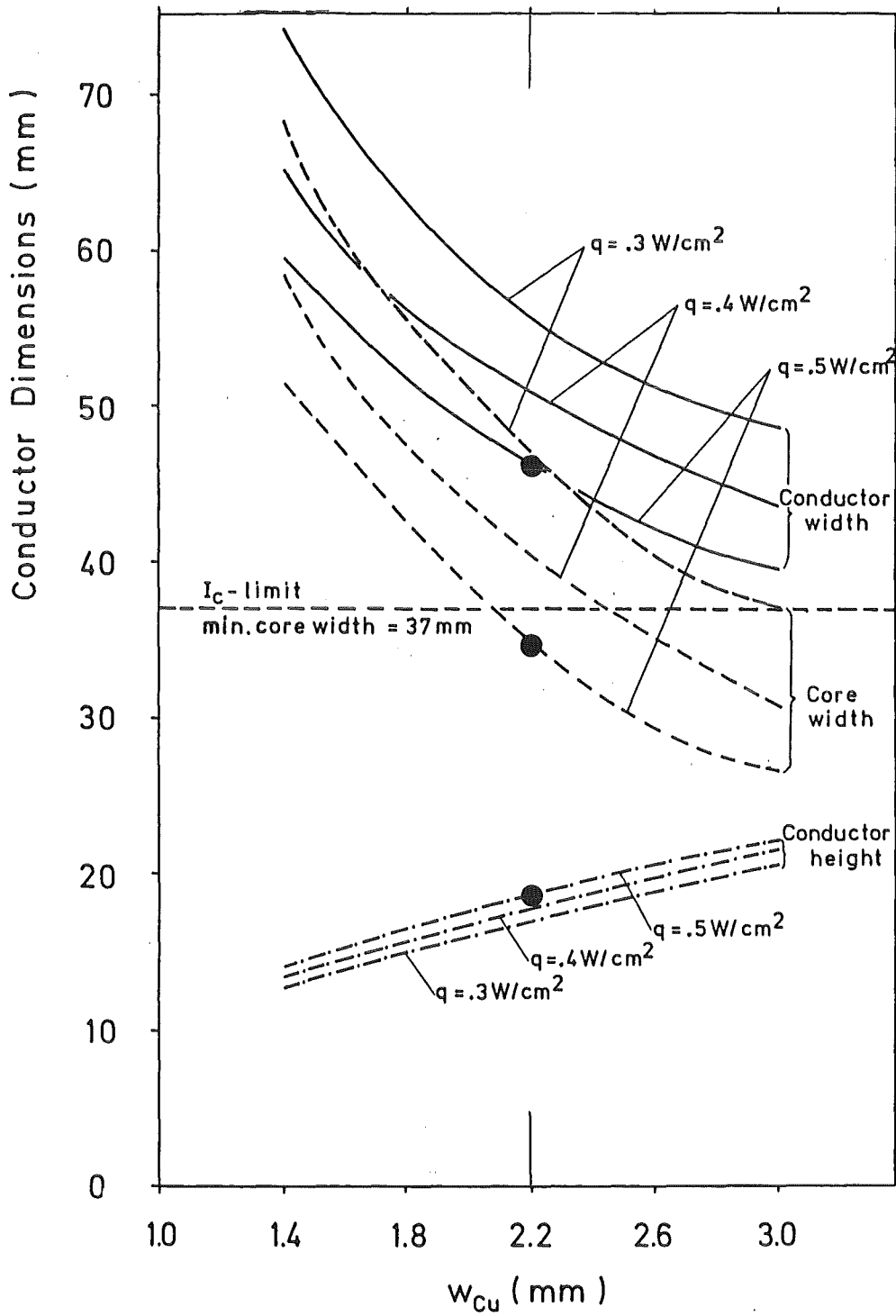
Fig. 3.7-1: Characteristic conductor dimensions vs. width of copper profiles for different heat flux densities into Helium. The I_c-limit on core width is valid for I_c (12 T, 4.2 K) = 30 kA. Core height (5.1 mm), copper fraction in core (12.7%), Helium channel width (1 mm) and aspect ratio of copper profiles (1.6) are kept constant. The points indicate the NET-II/KfK conductor.

3.7.4 Conductor performance

The main performance data of the NET-II/KfK conductor are summarized in Fig. 3.7-2. They are represented as four temperature curves along the 650 m length of conductor in a pancake:

- The critical temperature T_c of Nb_3Sn is approximated by $T_c[K] = 17 - \hat{B}/(2\ T)$ for the field region of concern (6 to 11 T as given in 3.2).

- The "current sharing temperature" T_s, i.e. the critical temperature at the operational current $I = 20$ kA, is again approximated by a simple interpolation which is sufficiently accurate for a rough design in a limited parameter range:

$$T_s = T_c(\hat{B}) - \frac{I}{I_c(4.2K,\ \hat{B})}\left[T_c(\hat{B}) - 4.2K\right] \text{ with}$$

$$I_c(\hat{B}) \cdot \hat{B} = 30 \text{ kA} \cdot 12 \text{ T} = \text{const.}$$

- The bulk helium temperature T_c is calculated with the program HEHT (see 3.6) taking into account helium flow losses at twice the friction coefficient of a straight tube, nuclear heating losses, time-averaged ac losses, and evenly distributed static loss of 10 W per pancake due to heat conduction and radiation from outside.

In accordance with 3.4.5 and the final conductor dimensions, the nuclear heating losses along the coil are given by

$$P_n(z) = 0.26 \text{ W/m} \cdot \exp(-z/120 \text{ m}) \quad \text{with}$$

z: coordinate along the length of conductor, starting at the inside.

The decay length of 120 m corresponds to five inner turns with a total radial thickness of about 9 cm.

In accordance with 3.5.7, the time-averaged ac losses are taken as 23.4 W per pancake or 36 mW per meter of conductor. Higher ac

losses are encountered in the outer windings close to the
PF coils. Therefore, a 3:1 variation of losses per meter is
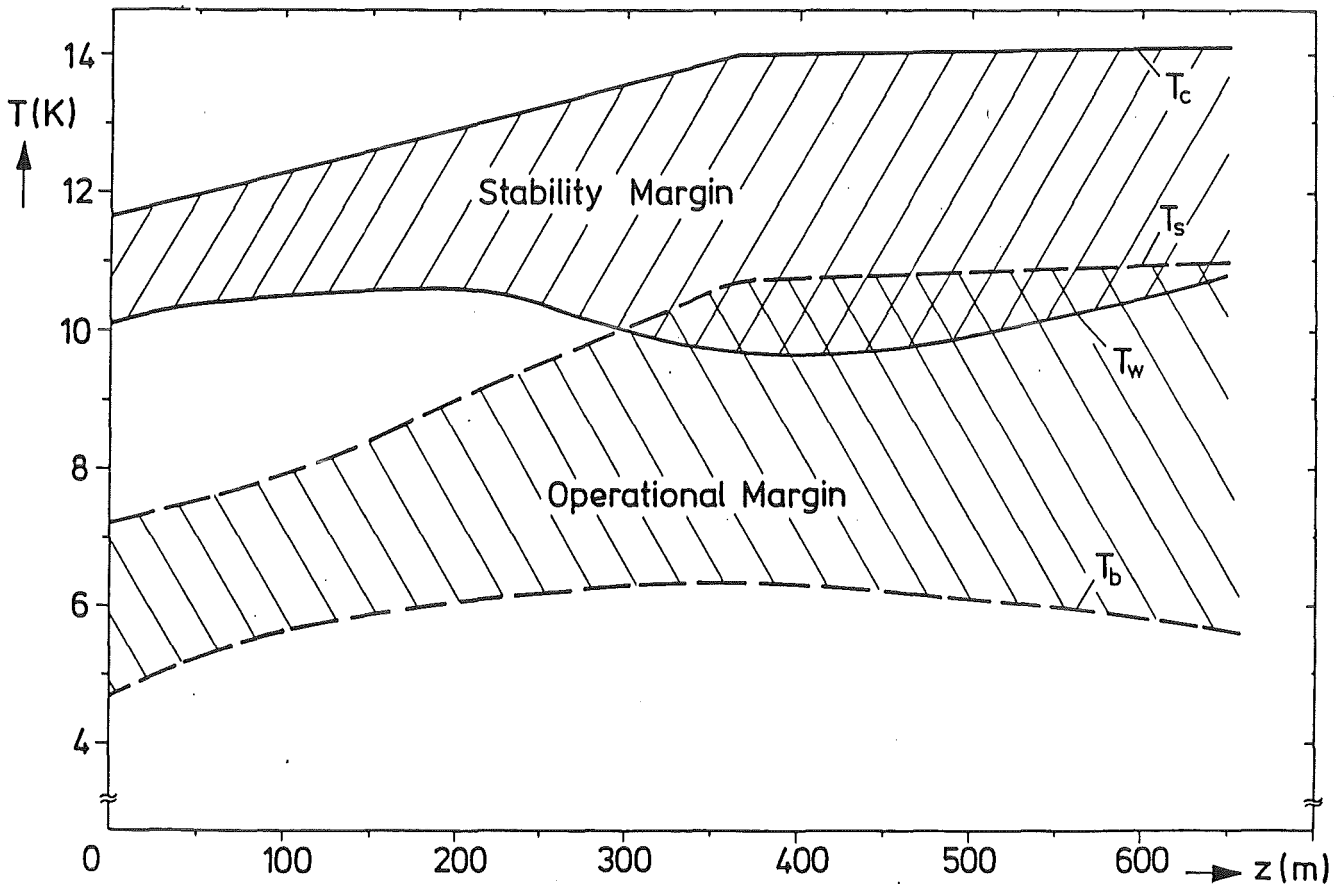
Fig. 3.7-2: Bulk helium temperature T_b, current sharing temperature T_s, critical temperature T_c, and metal wall temperature T_w along the conductor in a TF coil pancake.

assumed along the length of conductor. Including 15 mW per meter of static losses, one obtains

$$\frac{dQ}{dz} = P(z) = 0.015 \text{ W/m} + 0.018 \text{ W/m} + 0.036 \text{ W/m } z/650 \text{ m}.$$

The inlet temperature of the helium (4.7 K) is chosen to simplify the design of the cryogenic system and may be altered in a more detailed design. For reliable operation, $T_b(z) < T_s(z)$ is required.

- The wall temperature T_w is again calculated by HEHT, taking into account the heat transfer characteristics into forced flow helium as described in 3.6. The power density in copper in case of a "local" and "transient" normal conducting disturbance depends on the location in the winding due to the copper magneto-resistivity:

$$\mathcal{S}_{Cu}(B) = (1.08 + 0.46 \times \frac{\hat{B}}{1T}) \times 10^{-10} \, \Omega m.$$

The low field resistivity corresponds to a residual resistivity ratio of 150; at the peak field of 10.7 T, the resistivity amounts to $6 \times 10^{-10} \, \Omega m$. The conductor is designed to give a heat flux q of 0.5 W/cm^2 into helium with the peak resistivity value. With the field profile of Fig. 3.2-2, the resistivity dependence on z is given by

$$\mathcal{S}_{Cu}(z) = \begin{cases} 600 - 0.6 \, z \; 10^{-12} \, \Omega m & \text{for} \quad 0 \le z \le 364 \text{ m} \\ 380 \; . \; 10^{-12} \, \Omega m & \text{for} \quad 364 \le z \le 650 \text{ m} \end{cases}$$

The wall temperature T_w is finally calculated by

$$T_w(z) = T_b(z) + \frac{I^2 \cdot \mathcal{S}_{Cu}(z)}{A_{Cu} \, P_{met} \cdot h(z)}$$

The stability criterion chosen for a "local" and "transient" disturbance requires $T_w(z) < T_c(z)$.

Fig. 3.7-2 shows that the required conditions for operating temperature and stability against small disturbances are fulfilled.

In fact, compared to NbTi-conductors such as used in the LCT-coils, there are additional safety factors in terms of critical current, operating temperature, and probably even stabilization and Stekly parameter. However, they should only be built into a conductor design if more experimental evidence has been collected on conductors of this type and if the limits posed by mechanical loadings and safety (hot spot temperature, discharge voltage, quench detection) can be assessed more accurately.

The thermohydraulic parameters of helium flow are listed in Table 3.6-1 in addition to the key data of Fig. 3.7-2 as an example of the information obtained by the HEHT-program. The helium input parameters (initial temperature, initial pressure, mass flow) are selected to meet the operational and stability criteria at the least demanding values from the point of view of crygenic technology: Initial temperature of 4.7 K, initial pressure of 0.6 MPa, pressure drop to 0.29 MPa, mass flow of 5 g/s. With the heat losses assumed, the helium is in the supercritical state all along the conductor. The flow loss in a pancake amounts to $P_L = \dot{m} \, \Delta p / \mathcal{S}_{He} = 15$ W which is tolerable in view of 31 W of nuclear heating, 23 W of time-averaged ac-losses, and 10 W of additional static losses.

The conductor would also be capable of operating at higher losses. For a first glance, total losses of 250 W in one pancake were assumed ($P_N = 200$ W, $P_{ac} = 50$ W). They can be handled at $T_i = 4.7$ K, $p_i = 0.95$ MPa, $\Delta p = 0.65$ MPa, $\dot{m} = 8.5$ g/s which results in flow losses of about 40 W per pancake. In this case in which the nuclear losses outweigh the others, it may be advantageous to have the helium inlet at the outside to remove the bulk heat close to the outlet. This shows that nuclear heating losses of at least a factor of 5 higher could be tolerated at the expense of more complicated and costly cryogenics. Alternatively, larger ac losses can be conceived, e.g. to cope with a demanding vertical position control system or to remove the CuNi barrier between the core and the cryostabilizing region of the NET-II/KfK conductor.

The safety discharge requirements are usually summarized by the "hot spot criterion"

$$\frac{A_{Cu}}{A_{met}} \, j_{Cu}^2 \cdot \tau \;=\; \frac{I^2 \cdot \tau}{A_{met} \cdot A_{Cu}} = \delta_{Cu} \int_{4.2K}^{T_{max}} \frac{c_{Cu}(T)}{\rho_{Cu}(T)} \, dT$$

with A   = Area in conductor cross section,

    j_{Cu} = Operational current density in copper after a quench:

        $j_{Cu} = I/A_{Cu}$

    τ = Discharge time constant: τ = 2 W/($U \cdot I$) with W = stored energy, U = discharge voltage

    δ, c, ρ = Density, specific heat, resistivity.

It is assumed that the other metals have the same specific heat as copper. For T_{max} = 100 K and constant magnetoresistivity contribution of 5 x 10^{-10} Ω m to the resistivity of copper of RRR = 150, the right hand integral amounts to 4 x 10^{16} $A^2 s/m^4$.
With I = 20 kA, $A_{met} \cong 650$ mm^2 and A_{Cu} = 230 mm^2 we get

$$\tau = 2W/(I \cdot U) = 15 \text{ s or } U = \frac{2W}{\tau I} = \frac{2 \cdot 500 \text{ MJ}}{15s \cdot 20kA} = 3.4 \text{ kV}$$

Discharge voltages of the same order are used in LCTF, and much larger voltages are required for PF coil systems. Even this most conservative hot spot criterion turns out to be manageable. If cold end effects and transverse heat conduction are additionally considered, several seconds are available to discover and identify a disturbance in a coil as a "quench".

3.7.5 Pressure rise during the quench

The pressure rise in a long channel is often calculated by use of the formulae given in /20/. They assume that the channel is heated at a constant rate, and pressure builds up due to heating and decays due to a mass flow out of the ends. This pressure rise would be largest in the center of the channel. The conditions of /20/ are not applicable in our case because with the quench protection system, no constant heating source is available. Instead the LCT experiments have shown that during such a fast discharge only 2 percent of the stored energy, W, were dissipated in the coil. A similar number results if one assumes that a pancake is completely normal conducting at a temperature of 70 K during the safety discharge. Its resistance would be

$$R = \frac{\rho_{Cu}(70 \text{ K}) \times L}{A_{Cu}} = \frac{1.5 \times 10^{-9} \, \Omega\text{-m} \times 650 \text{ m}}{230 \text{ mm}^2} \approx 4 \text{ m}\Omega$$

This is roughly 2 % of the value of the discharge resistor of 290 m for 5.8 kV at 20 kA.

Therefore, another approximation for the quench pressure should be used for the NET coil.

Two pessimistic assumptions can be made:

- the energy 0.02 W (W = stored energy) is dissipated only into one hydraulic path (one pancake),
- the helium within this path is heated at constant volume (both ends closed).

This process heats the coil to the temperature T_{max} which is given by

$$\int_{T_o}^{T_{max}} (M_{He} C_{V,He} + M_{Met} C_{Met}) \, dT = 0.02 \, W$$

Assuming the total stored energy W = 1100 MJ and the metallic and helium masses of $M_{He} \approx 11.2$ kg/pancake and $M_{Met} = 3200$ kg/pancake, respectively, the resultant temperature becomes

$$T_{max} \approx 80 \, K$$

During isochoric heating the helium pressure would increase to

$$P_{max} \approx 200 \, bar$$

This shows that the quench pressure will not be a serious problem if the system is actively quench protected in such a manner that a fast discharge is initiated as soon as a predefined resistive voltage is exceeded in any single pancake.

4. Cooling needs and refrigeration

The 16 pancakes of the coil will be cooled in parallel with a mass
flow of 5 g/s each. Taking into account heat loads according to
chapter 3 inlet conditions of 6 bar and 4,7 K are proposed. The high
critical temperature of the superconductor permits use of a 4.5 K/1.3
bar LHe bath for heat exchange with the supercritical helium. This
gives the advantage to realize easily positive pressure inside the
whole cooling system and to exclude air contamination problems.
Supercritical cooling of the coil at a low pressure level with a
pressure of 6 bar at the inlet of the coil keeps small the necessary
refrigeration capacity due to helium operating conditions close to
the "Inversion-line" (boundary between negative and positive JT
effect). So the mass flow of 5 g/s in the pancake is sufficient to
keep the temperature at the outlet of the coil below 6 K (5.7 K). At
low pressure levels a refrigeration configuration with a closed
secondary loop and a cold helium circulator in comparison to a direct
cooling with the refrigerator flow becomes attractive: Beside the
operation flexibility "independent" of the refrigerator mass flow and
the "hydraulic" decoupling of the coil system from the refrigerator
an acceptable overall cooling efficiency can be expected (Fig. 4.-1).

This first calculation of the refrigeration capacity necessary to
cool the coil has been done for a cooling system with a closed
supercritical secondary loop using a LHe-pump and a LHe heat
exchanger bath for thermal coupling with the primary loop. The
cooling capacity must be sufficient to remove the heat loads and
amounts to approx. 2.2 kW at 4.5 K (Fig. 4-2).
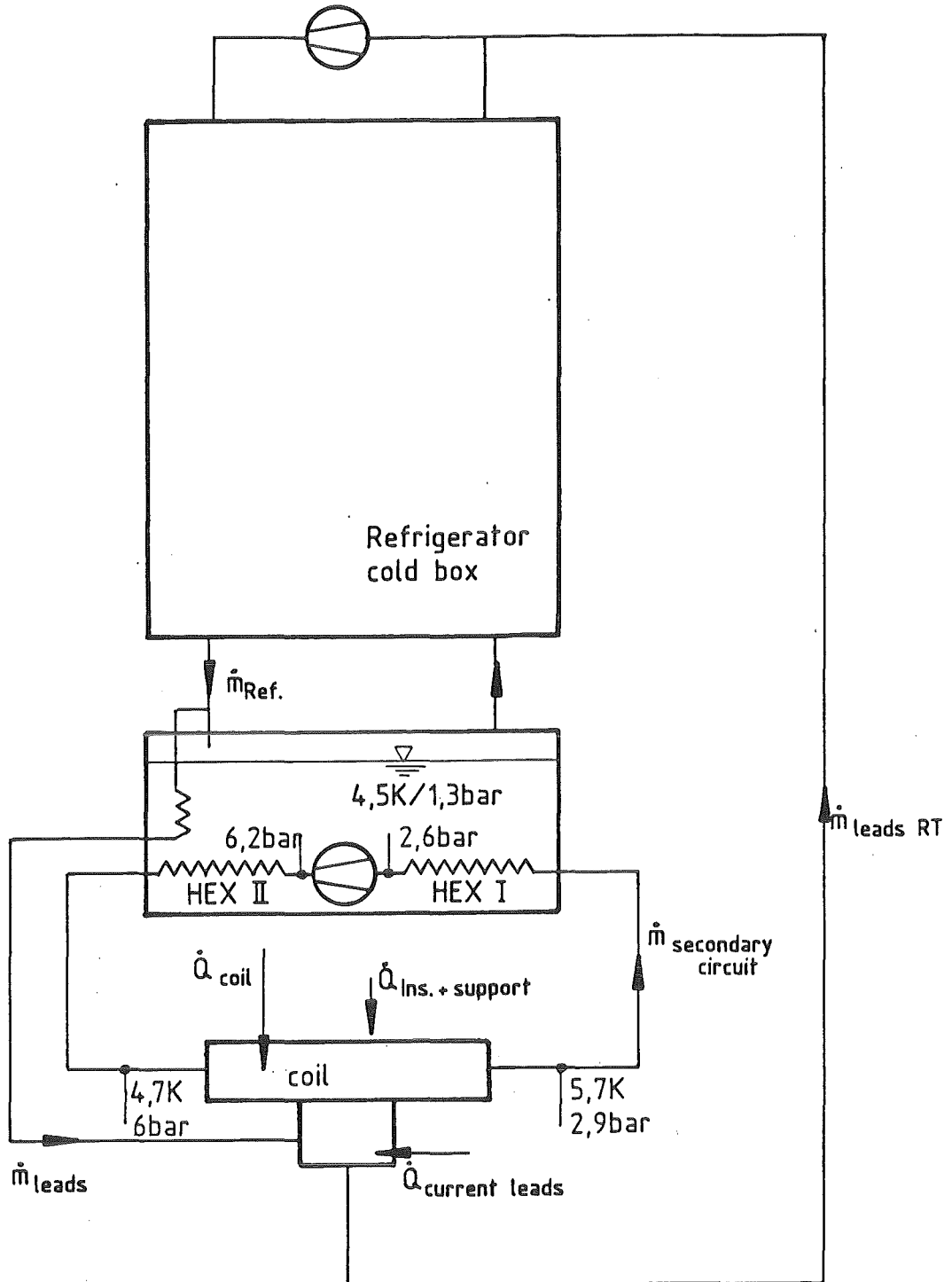
Fig. 4-1: Cooling principle with the refrigerator and the closed secondary
cooling circuit for the coil

The calculation is based on cautious assumptions for the efficiencies of the cold He pump and the current leads (extrapolated from first 10 kA-LCT-experiences). A safe calculation of the heat load due to thermal insulation and mechanical support demands for a detailed engineering design of the coil system and cryostat.

At the operating conditions indicated (see also Fig. 4-1) the transposed critical line is only crossed near the outlets of the 650 m long pancake-cooling channels under stationary conditions and may be under transient normal conducting zone conditions. Density wave oscillations due to large expansion effects in the coolant can be avoided according to experimental investigations at NBS Boulder with a heated circular pipe /22/.

Cooling down of the coil has to be done directly with the refrigerator mass flow in a temperature controlled manner mixing warm gas of the compressor with cold gas of the coldbox.

$\dot{Q}_{aeq. 4,5K}$ (W)

	Σ 2 265	100%
Current leads 20 kA	500	22%
Thermal insulation and mechanical support	150	7%
HEX I + HEX II He-Pump ($\eta_s = 0,5$)	495	22%
Coil (friction, AC losses, nuclear load, static losses)	1 120	49%
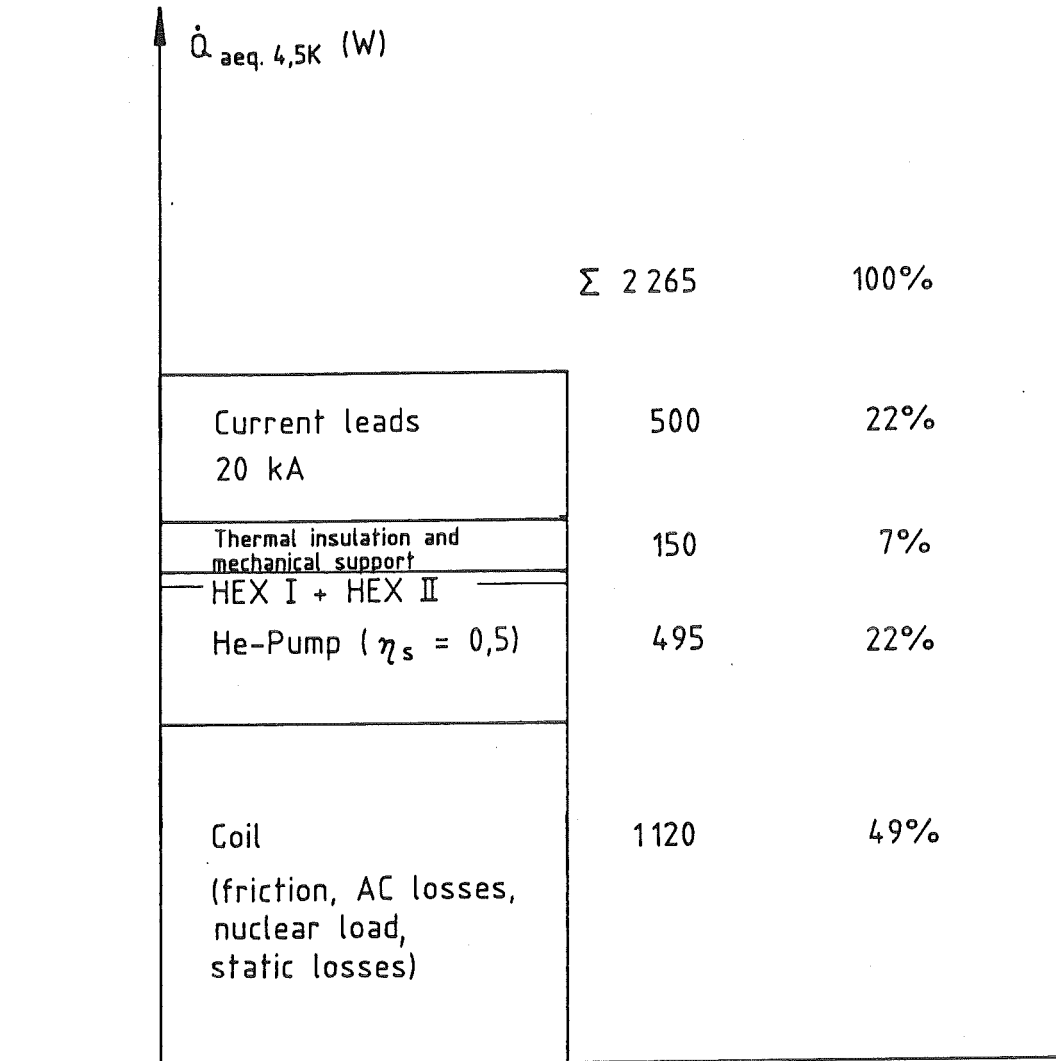
Fig. 4-2: Heat loads of the coil to be refrigerated

5.   Fabrication steps

A detailed study of the fabrication steps for each component of the
conductor shows that a multitude of details have still to be opti-
mized by experimental investigation, actually under work at KfK. In
the following, more precisions about the fabrication steps of various
conductor components is given, demonstrating the feasibility of each
one of these components based on the present state of the art . In
practice, economical aspects will lead to a combined processing of
various steps rather than to the independent processing of each step,
thus creating additional difficulties. An example of such combined
processing is the "roebling" of Cu profiles on the core without
damaging the reacted Nb_3Sn strands. In this case, a careful analysis
of the working data collected during the fabrication of the Euratom-
LCT coil was necessary before an optimistic consideration of the
problem was arrived at.

5.1   The core

The internal core consists of the folded insulation strip, the Nb_3Sn
cable and the CuNi barrier.

5.1.1   The folded insulating strip

The function of the folded strip is the same as in the Euratom/KfK
conductor: it must ensure a high resistivity between the two Nb_3Sn
strand layers, thus leading to considerably lower ac losses. This is
achieved by cabling the 36 Nb_3Sn strands around a strip with a high
resistivity between the two flat surfaces. For this purpose, a very
thin (~0.1 mm thick) foil of stainless steel or Cu-Sn bronze is
folded around an insulating ribbon, woven with thin ceramic fibers.
Such "flexible" ceramic tapes are commercially available.

Own experiments show that these tapes withstand the reaction heat
treatment without major damage. Further experiments have to be done
in order to ensure that the deformations arising during the
calibration operation do not degrade the insulating properties.

5.1.2   The Nb$_3$Sn cable

36 circular Nb$_3$Sn strands of 1.92 mm diameter (see specification in 2.2) have first to be cabled with a transposition length of 330 mm around the central strip.

A serious problem when cabling this assembly is the "spring" effect of the bronze, which is even present after a recovery annealing at $\sim$ 500 C. Previous experiments have shown that the problem is considerably reduced by a plastic deformation of the strands just after cabling. Prior to the reaction heat treatment, the assembly folded strip + Nb$_3$Sn cable is thus calibrated to the external dimensions 4.3 x 36.0 mm^2 .

At this stage, the thickness of the strands would be 1.8 mm, leading to the deformed shape shown in Fig. 2.2-2. The effect of the intimate electrical contact between neighbour strands is attenuated by the high resistivity of the external bronze (ρ_{Br} = 3.2 x 10^{-8} Ω m).

At this level, the remaining voids to be filled by solder occupy 4.1% of the total cross section (Table 2.3), the distance between the flat bronze surface and the CuNi barrier being 0.1 mm. The present calculations have been performed with these dimensions, although a slighty stronger reduction by calibration, leading to a smaller "lost" cross section, occupied by solder and voids would also be possible. If necessary, the content of the voids between Nb$_3$Sn strands and central strip could be lowered to $<$ 1 % of the conductor cross section.

The most delicate operation is the reaction heat treatment and the following manipulations. Experiments at KfK with prereacted Nb$_3$Sn wires for the HOMER facility have shown that the positioning during the reaction heat treatment has to be extremely careful.

In order to keep the Nb$_3$Sn strands together as close as possible a strong mechanical guidance must be provided during the reaction heat treatment. For this purpose, the assembly strip + Nb$_3$Sn for each pancake ($\sim$ 650 m length) would itself be wound to a pancake of 3 m internal and $\sim$ 5 m external diameter (R$_o$ = 1.5 m, see Fig. 3.3-1).

The winding of this pancake would be very tight: in order to prevent contact between the Cu bronzes of two neighbouring turns (sintering!) a steel tape with ceramic insulation has to be inserted. The most important problem in building a reaction furnace of $\emptyset_{ext}$ 6000 mm consists in ensuring a good temperature homogeneity, of $\Delta T = \pm 10$ C. The thickness of the furnace could be adapted to the number of pancakes to react simultaneously, and could reach e.g. 500 mm for 4 pancakes. During the reaction heat treatment, the pancakes have to be set <u>horizontally</u>, in order to equalize the gravity effects throughout the whole cable length. An important point is the guidance of the reacted Nb_3Sn cable after leaving the furnace: a smooth movement through well-defined leading rails is required.

The technique illustrated in Fig. 5.1-1, where the Nb_3Sn strands are reacted on a horizontal spool ($R_o = 1.5$ m), straightened and wound
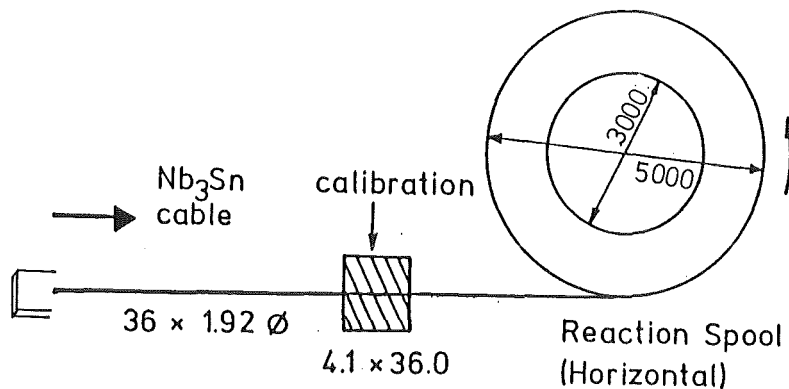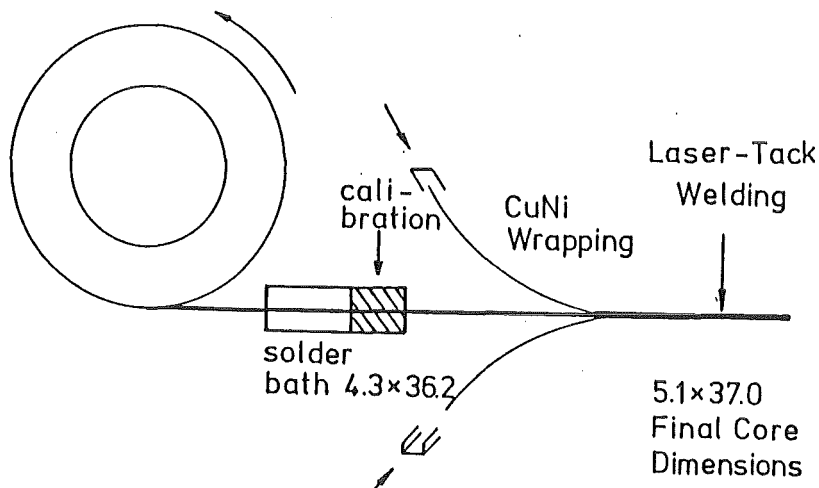
Fig. 5.1-1: Production line for the core (all dimensions are in mm)

again to the final coil size has been applied in several systems, e.g. in Japan for the cluster test facility (TMC-I and TMC-II) and at KfK (Homer). It can thus be considered as feasible, the only really new condition being the large coil size. In all these cases, the really important boundary condition to fulfill is the strictly synchroneous movement of both, the spool with the reacted Nb_3Sn and the NET pancakes, thus necessitating very careful control.

5.1.3 The CuNi barrier

The CuNi barrier between the Nb_3Sn strands and the Cu profiles is soldered to the former after the reaction heat treatment. The CuNi barrier being very thin (the design value is 0.4 mm), the wrapping operation is expected to be possible without damage for the reacted Nb_3Sn strands. Since no calibration can occur on reacted Nb_3Sn strands, the surface of all four CuNi sides must be very smooth in order to permit the soldering of the Cu profiles with low solder thickness, < 0.1 mm. This can only be realized if the operation of mounting the CuNi barrier immediately preceeds the Roebel process, i.e. the cable is maintained straight during the operations following unwinding of the reacted Nb_3Sn spool.

After unwinding the reacted spool, the Nb_3Sn cable is driven through a solder bath and is subsequently driven through a rectangular die-block with the dimensions $4.3 \times 36.2 \ mm^2$. For this purpose, the temperature of the die (a ceramic die for preventing reaction with the solder) decreases gradually in the drawing direction, the inlet being at a temperature slightly above the melting point of the solder. This operation is mainly necessary for filling the external voids (shown in Fig. 2.2-2) with solder. The solder thickness between the strand surface and CuNi being in each case < 0.1 mm.

The CuNi barrier is mounted starting with two CuNi tapes with different widths, 36.2 mm (long side of the core) and 46.4 (long side + 2 short sides of the core). The broader tape is deformed to an U shape of the final core dimensions, $5.1 \times 37.0 \ mm^2$ and is placed around the calibrated Nb_3Sn cable. Simultaneously, the narrower CuNi tape is placed on the top of the conductor (see Fig. 5.1-2), after which both tapes are laser-tack-welded with one weld spot each few centimeters. This operation is necessary in order to ensure a precise

welding spot

CuNi barrier

Rounded Corner

Nb_3Sn cable

5.1

37.0
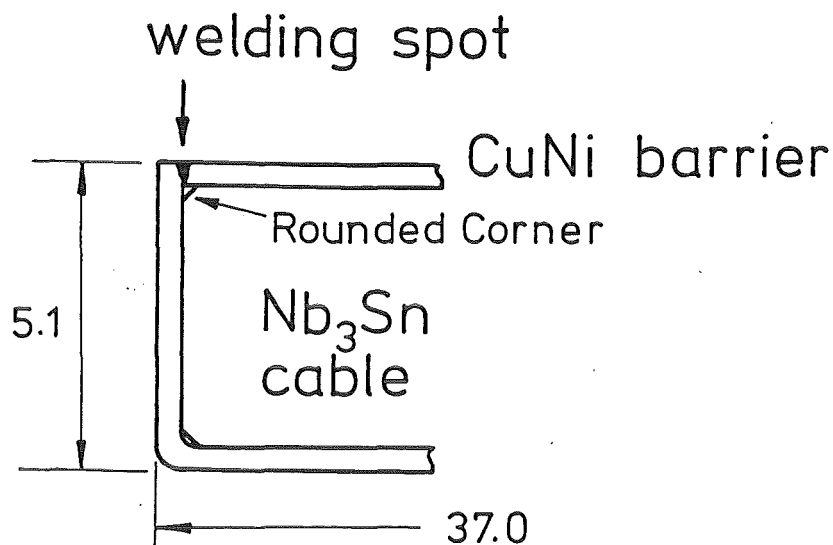
Fig. 5.1-2: Detail of core fabrication

positioning of the external core dimensions during the following
soldering procedure of the Cu profiles on the core. In order to avoid
contact between molten CuNi and the solder at the weldments, the
corners of the Nb_3Sn cable could be rounded off during the
calibration procedures (see Fig. 5.1-2).

5.2   The cryostabilizing region

The cryostabilizing region, situated between the core and the steel
conduit, comprises 26 Cu profiles, separated by He channels. The Cu
profiles (3.6 x 2.2 mm^2 cross section) are mounted by the Roebel
process with a transposition length of 1 m (see Fig. 5.1-3). From the
Euratom LCT coil, it is known that the Roebel process allows to
maintain such small distances as 0.9 mm between the Cu profiles (1.0
mm for NET-II). The longer transposition length (1 m compared with
40 cm for Euratom LCT), was chosen for avoiding electrical contacts
between neighbouring Cu profiles at the corners, which would lead to

seriously enhanced ac losses. The aspect ratio 1:1.6 for the Cu
profiles has been chosen especially for meeting the Roebel require-
ments.
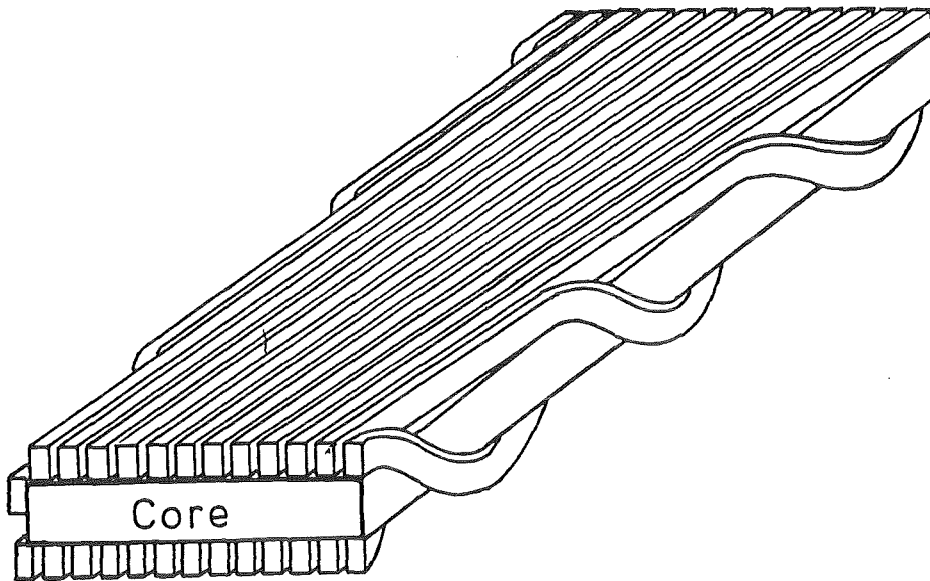
Fig. 5.1-3. The Cu profiles after roebling around the core.

The mechanical deformation resistance of the Cu profiles will be
similar to that of the Cu-NbTi strands in Euratom LCT. An important
difference, however, concerns the surfaces of the Cu profiles which
have to be treated in the case of NET-II/KfK conductor.

a) the narrow sides are plated with solder prior to roebling ($\sim$ 0.05
   mm thickness). This thickness permits optimal soldering after this
   process, avoiding solder bridges between neighbouring Cu profiles,
   which would again lead to enhanced ac losses.

   It has to be noted that since the broader sides of the Cu profiles
   are not solder coated, they are soldered to the core at its
   broader surface only, covering 88% of the total length.

b) the broader sides of the Cu profiles can be treated by sand-
   blasting or other processes in order to increase the surface. The
   present calculations have been undertaken without this beneficial
   effect, which would result in an enhanced safety margin or even in
   a larger overall current density.

5.3   The steel conduit

The considerable thickness, 2.45 mm, of the steel conduit for NET-II
requires a particular type of conduit fabrication. This thickness
causes some problems which can be summarized as follows with respect
of U-shaping of the conduit:

- folding of a steel tape to an U-profile results always in rounded
  off edges at the corners of the profile.
- the necessary radius at the corner increases with the thickness of
  the tape material
- the decreasing of the U-profile height sets fabrication limitations
- the rounded off edges are disadvantageous for the transverse
  transmitting forces. Bending stresses may result with such rounded
  off geometry in the conduit material, which should be avoided
- The U-profile fabrication must be integrated in the assembly line
  of the cable production. A non-integrated fabrication means that
  the U-profiles must be spooled, which may result in additional
  geometrical distortion of the U-profile configuration.

Out of these points the search for an alternative way was indispen-
sable. The solution as given below (see Fig. 5.3-1) is independent of
conduit thickness, the thickness limitation being only given by the
requirement of a distortion free welding process. It could even be
employed in a conductor and coil design which carries the centering
forces and does not require an additional vault.
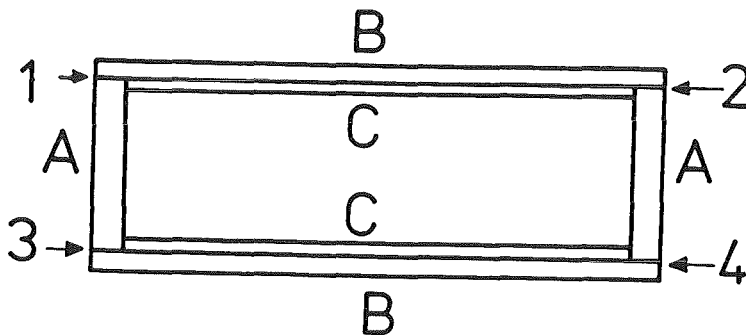
Fig. 5.3-1 Fabrication of steel conduit with tapes A, B and C.

The fabrication of the individual tapes A, B and C with exact
tolerances is possible. The joining C to B can be done by EB tack
welding (as in the case of Euratom/LCT coil) or by laser beam
welding. Today, the latter one is considered as being more economic,
because out of welding. The tapes A and B/C can be spooled on and off
in standard way without any distortion. Therefore an integration of
the fabrication steps in the cable production is not necessary. The
welding of the positions 1, 2, 3 and 4 can be done by laser
processing, which allows welding of I-type joints. It follows that
the core will be carefully treated during this operation. In
particular, tapes C protect the conduit interior during the welding
process. The NET-II/KfK conductor with the weldments of the steel
conduit is shown in Fig. 5.3-2 (similar to Fig. 2.2-3).
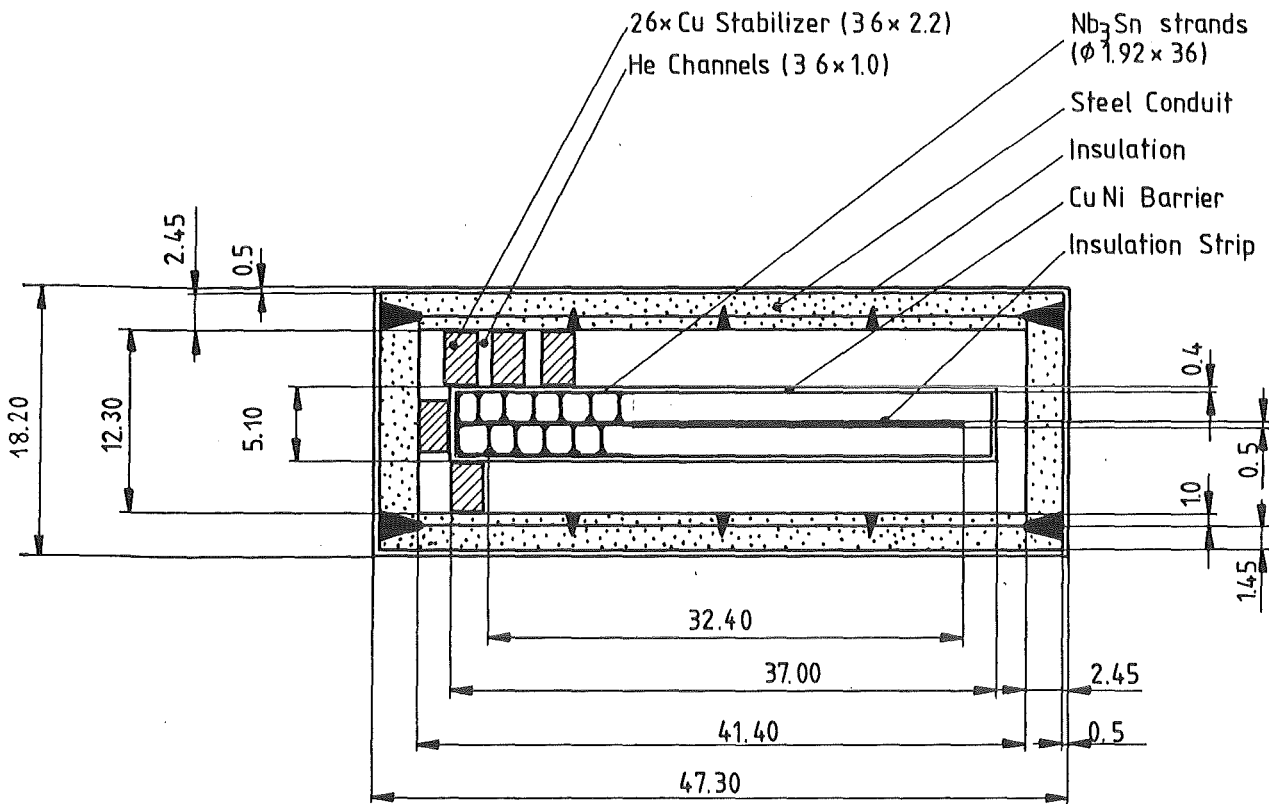
Fig. 5.3-2. NET-II/KfK conductor, showing the weldments of the steel
conduit.

Material choice for the steel conduit

Taking the results of mechanical calculation the compressive stress
in the conduit section (A) is   130 MPa. Cryogenic structural
materials such as 316 LN can easily withstand this compressive force.

The tensile yield strength of 316 LN is 1100 MPa at 4 K, a high
safety margin is therefore already existent. The laser beam
weldability is also already demonstrated (see also Chapt. 6.3). It
follows that this material, already used in the Euratom/LCT coil, is
suitable for steel conduit fabrication.

5.4   The insulation

The insulation tapes (PG-10CR) will be wrapped around the steel
conduit. After the wrapping process organic polyimid /30/ resin will
be applied in order to keep in place the insulating tapes during
pancake winding. Between pancakes, insulation plates of the same
insulation material are foreseen.

5.5   Quality control considerations

For obvious reasons the ultimate proof for the sound performance of a
fabrication length of a superconductor at operational temperature
cannot be given prior to cooldown and operation of the magnet into
which the conductor is wound. No complete and continuous conductor
test at superconducting temperature seems to be technically and
economically conceivable. Concerning for example the current carrying
capacity, critical current measurements are performed on short
samples, taken from each end of a conductor length. For high current,
high field conductors like the NET-II conductor even this procedure
seems to be prohibited due to the involved cost and time. This fact
is not so unsatisfactory for cabled conductors as it would be for
monolithic conductors, because of the possibility of current sharing
between the strands in case of some damage of a few individual
strands. Cable critical currents probably will only be measured on
some samples and the routine critical current measurements will be
restricted to the strands.
Above described situation is most pronounced for the critical current
but is of course also true for other electrical properties (e.g.
residual resistivity of the stabilizer) and for the mechanical
properties. A carefully worked out quality control system is there-
fore required to guarantee a constant quality of the conductor over
its whole length.

As for the superconducting strands much progress has been made with respect to continuous quality especially by those manufacturers producing wires for nuclear magnetic resonance spectroscopy (NMR) and imaging (MRI), mainly for NbTi but also for bronze route Nb_3Sn conductors. The magnets built for this application are operated in a persistent mode so that wires with very constant properties are required to avoid any resistivity (e.g. due to inhomogeneities or broken filaments) and to allow for low field decay rates. The key to the reliable fabrication of such conductors is to find out and to control the relevant influence parameters. Examples are the strict specification and control of starting materials (Nb, CuSn, Ta, Cu) with respect to chemistry, homogeneity, cleanliness, surface conditions and electrical and mechanical properties in conjunction with the control of the process parameters during fabrication of the conductor. Examples for powerful non-destructive tests are ultrasonic inspection and eddy current testing for the starting materials and for the strands at intermediate and final dimensions. As the requirements on homogeneity and low resistivity are much smaller for the NET conductor than for an NMR conductor, it seems that the established quality standard for the bronze type Nb_3Sn strands is more than adequate for NET application.

Leaving apart for the moment the reaction treatment for the formation of the Nb_3Sn as well as the handling of the reacted conductor with the brittle A15 phase, most of the envisaged subsequent manufacturing steps are essentially state of the art and are proven by the successful operation of magnets with flat cables and especially the Euratom/LCT coil:

- fabrication of the flat cable ("Rutherford" cable)
- solder filling of the cable
- Roebel-type application of the stabilizing elements including the continuous soldering process
- Conductor sheathing and final seal welding

The procedures developed to assure the constant quality of these cabled and sheathed conductors consist mainly in the control of the relevant process parameters like conductor cleanliness, fabrication speed, temperatures, forces and geometry. They seem to be also

adequate for the NET conductor. The same is true for the established methods to determine the parameters of the intermediate products and the final conductor (geometrical dimensions, leak tightness, hydraulical properties). Samples taken from the ends can be used to verify directly some important performance characteristics not accessible by continuous test methods (e.g. by bending tests).

As already indicated above, there still exist two fields where more experience is required before an adequate quality control system can be established. The first aspect is related to the reaction treatment of the Nb_3Sn conductor in the required large quantities (e.g. control and homogeneity of the temperature-time cycle). The second concerns the handling of the brittle A15 material in an industrial environment during all subsequent conductor fabrication steps and during coil fabrication (e.g. degradation due to straining and establishment of adequate safety margins). At present, the knowledge in these fields increases gradually with the ongoing development projects but will be significantly enhanced for conductors with NET-relevant size and geometry.

5.6 Approximate costs

At present, it is very difficult to predict with some accuracy the production costs of a conductor which is not well developed yet. For the special case of the present conductor concept it is helpful that some fabrication steps are similar to those in the Euratom/LCT conductor, where the costs are known.
Another uncertainty still subsists about the costs of the Nb_3Sn strands, where first numbers from industry have just been obtained.

Thus following cost breakdown for the conductor can be given:

a) Conventional materials/ components	amount/conductor unit length (kg/m)	costs/conductor unit length (DM/m)
Steel conduit	2,0	20
Cu profiles	2,0	40
CuNi tape	0,3	45
Ceramic ribbon	0.065	12
	=	117 DM/m

b) Nb₃Sn strands

A specific price of 60 DM/kAm at 12 T is quoted for standard strands with about 25% Cu as fabricated by the bronze route. If one takes into account a 25% price reduction for the huge amount of strand material needed for NET, the costs for the strands of the conductor under investigation in this study will be

$$60.-- \text{ DM/kAm} \cdot 30 \text{ kA} \cdot 0,75 = \underline{1350 \text{ DM/m}}$$

c) Manufacturing costs

Each one of the two major steps, namely

- cabling of Nb₃Sn strands + reaction + soldering and covering with CuNi, and

- Cu profile roebling on the core + soldering + encapsulation by the steel conduit,

is individually roughly equal to the LCT manufacturing process. This process had costs of about 500 DM/m, so that for the NET conductor at least 1000 DM/m must be calculated.

d) Total conductor costs

In addition to the items a) - c) about 10% additional costs should be considered for further quality assurance and inspection. Thus the total costs of the NET-A15-conductor will be in the order of

$$\underline{2700 \text{ DM/m}}$$

This corresponds to specific costs of 0.09 DM/Am, which has to be compared with 0.056 DM/Am for the Euratom/LCT conductor (NbTi, 8 T only) and seems therefore reasonable.

6.   Conductor Development and Test with KfK Facilities

The requirement of high critical currents in a NET conductor, combined with the presence of a strong reinforcing structure has raised the question about the highest limits attainable with Nb₃Sn. The study of these questions is part of an extended material research program at KfK.

6.1   Optimization of the Nb$_3$Sn strands

In the last years, various additives to Nb$_3$Sn have considerably

increased J_c in the field range above 11 Tesla. The question of

interest was to know what additive would cause the highest increases

of J_c . For this purpose, a series of Nb$_3$Sn wires with different

additives has been prepared by the bronze route.

The wires contained 19 or 361 cores, and the geometrical dimensions

were chosen to be identical, in order to obtain a meaningful

comparison. The critical current densities of these wires (taken for

the A15 layer) are presented in Fig. 6.1-1 for fields up to 23 Tesla

/23/. It is seen that the best J_c values for the three additives Ta,

Ti and Ni + Zn are almost identical up to the highest measured fields

(Ti, Ta and Ni were added to the Nb core, Zn to the Cu bronze). It is

seen that J_c of binary Nb$_3$Sn wires exceeds that of ternary wires at

fields below 11 Tesla. The maximum field in the actual NET design is

thus just situated at the crossover between both curves.
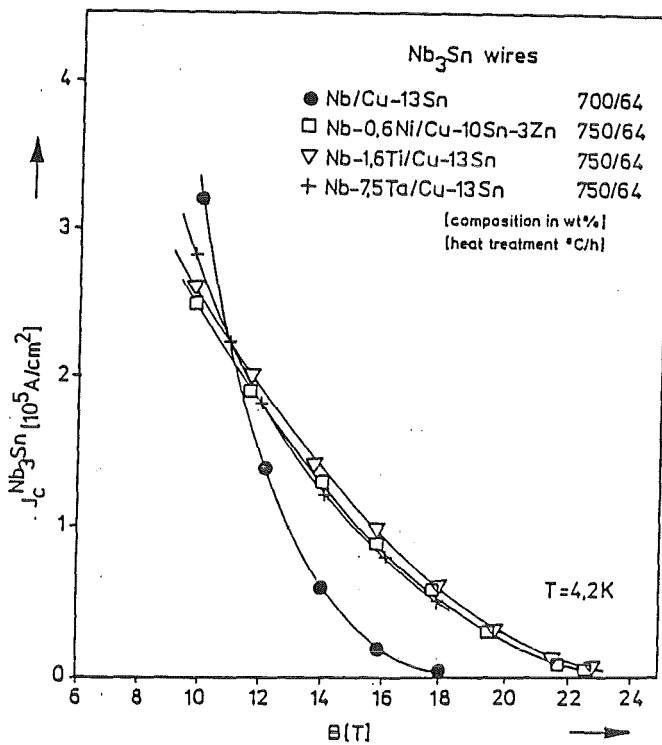
Fig. 6.1-1   Critical current densities in the Nb$_3$Sn layer as a
             function of the magnetic field for a series of 19 core
             wires with and without additions /23/

The corresponding extrapolation of the upper critical magnetic field, B_{c2}^* shows clearly an increase from 21 T to 24 - 25 T, i.e. of 3 - 4 Tesla, independent of the nature of the additive /23/.

The effects of additives on J_c and B_{c2} of Nb_3Sn wires can be understood as follows: Nb_3Sn is a perfectly ordered system (the order parameter was recently determined at KfK to S = 1), and the electrical resistivity, just above T_c, ρ_o, is very low: 16×10^{-8} Ωm. The additives act as a small perturbation of this perfectly ordered state, leading to a reduction of the electronic mean free path and thus to an increase of ρ_o. Recently, an increase up to $\rho_o \approx 35 \times 10^{-8}$ m was found /24/, which is sufficient to explain the observed increase in B_{c2}^*. Since $B_{c2}^* \sim T_c \cdot \gamma \cdot \rho_o$ and T_c and γ are essentially unchanged by the effect of additives, the increase of ρ_o is mainly responsible for the enhancement of B_{c2}^*. The increase of ρ_o in fully reacted Nb_3Sn filaments with and without additives is represented in Fig. 6.1-2.
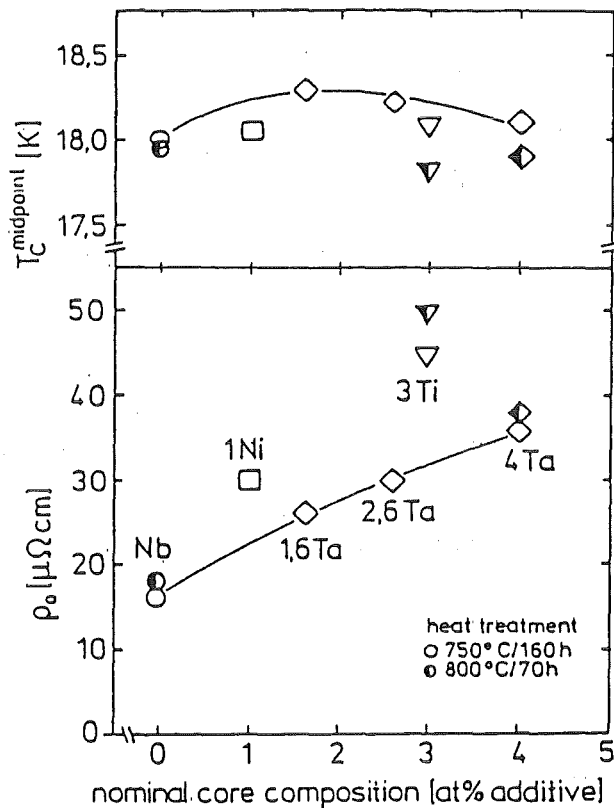
Fig. 6.1-2 Residual resistivity and critical temperature for unalloyed and Ta, Ti and Ni+Zn alloyed Nb_3Sn filaments as a function of nominal concentration of core additive for heat treatment at 750^oC /24/.

The independence of the chemical nature of the additive on the enhancement of J_c leads to an important conclusion, which also holds for Nb_3Sn wires prepared by other techniques than the bronze route:

- It is not longer necessary to search for new additives. It seems that the highest limits of J_c at high fields as caused by additives in Nb_3Sn wires have been reached. Further improvements can only be reached by improving the pinning mechanism.

There are indications that the newly developed "internal Sn diffusion" technique leads to considerably higher values of J_c around 11 T. Further, it is not known whether pinning in alloyed Nb_3Sn can be improved: at present, it is too early to decide between binary or alloyed Nb_3Sn (with Ta or Ti as possible additives) for the NET-II conductor. This will also depend on the results of stress sensitivity of J_c in NET-like conductors, where the measurements will not only comprise axial, but also transversal stresses.

6.2   Strain behavior of J_c in Nb_3Sn wires

6.2.1 J_c vs. $\mathcal{E}$ for alloyed Nb_3Sn wires

The effects of precompression on the critical current density, J_c, of Nb_3Sn wires are known up to 23 T. At 12 T, the decrease of J_c of a bronze-processed binary Nb_3Sn wire with $\mathcal{E}_m = 0.3\%$ is of the order of 30%. For alloyed Nb_3Sn wires, the decrease of J_c with precompression was found to be smaller with respect to that encountered for binary wires. A research program, undertaken at KfK in order to determine the effect of alloying on the stress sensitivity of J_c yielded the results shown in Fig. 6.2-1 /23/.
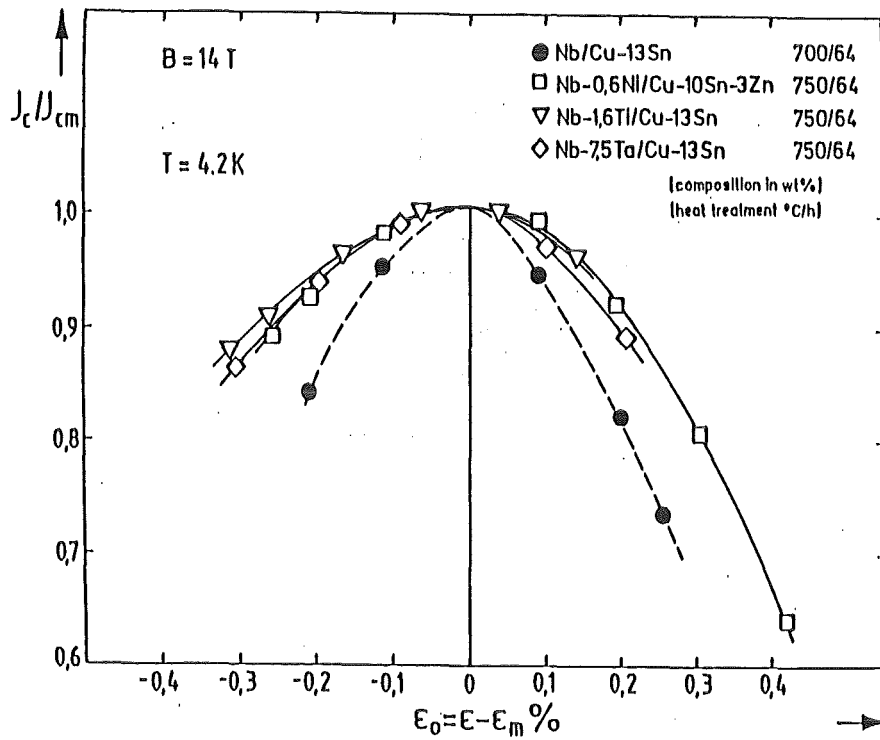
Fig. 6.2-1: Strain dependence of J_c binary and ternary Nb_3Sn wires
/23/.

It is seen that the strain sensitivity of ternary Nb_3Sn wires is
reduced when compared with that of binary Nb_3Sn, which is mainly a
consequence of the enhancement of B^*_{c2} (The reason for the variation
of J_c with the strain is due to hydrostatic and nonhydrostatic
pressure gradients, which also cause crystallographical changes in
the originally cubic A15 structure).

The effect of a simultaneous reaction heat treatment of reinforced
binary and ternary Nb_3Sn wires /25/ is shown in Fig. 6.2-2. In
particular, the precompression resulting from austenitic steel is
0.9%. Again, the strain sensitivity of J_c is smaller for ternary
Nb_3Sn wires.
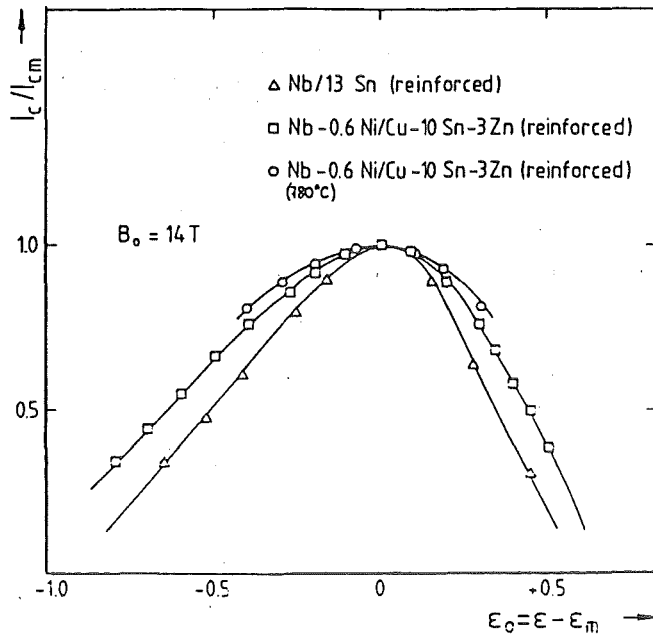
Fig. 6.2-2: Strain dependence of J_c in reinforced binary and ternary
Nb$_3$Sn wires (austenitic steel) /25/.

In order to reduce the precompression on the Nb$_3$Sn filaments, we have
replaced the steel by Inconel or by Mo (see Fig. 6.2-3). For Mo, it
was found that the whole precompression was compensated, in virtue of
its very low thermal expansion coefficient /26/. Obviously, a con-
ductor without any precompression would exhibit higher J_c values but
would not be very useful since the Lorentz forces would put the
filaments under a tensile load, possibly causing filament fractures.
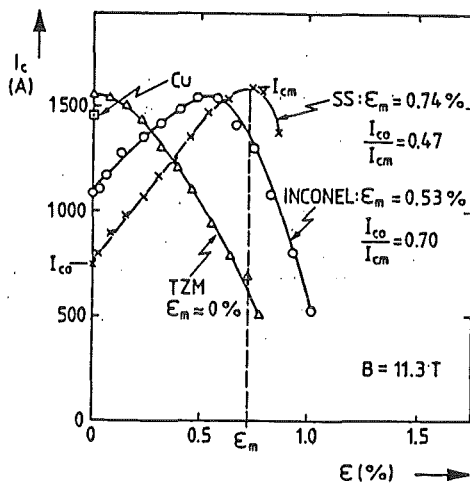
Fig. 6.2-3: J_c vs. ε for the same Nb$_3$Sn monolithic wire after
reinforcement by steel, Inconel or Mo (TZM is essentially
Mo with 0,5% Ti and traces of Zr and C) /26/.

For this reason, we have tried to substitute the amount of steel by
a certain volume fraction of Mo. As a result, it has been possible to
obtain reinforced wires with exactly the same degree of precompres-
sion as in the unreinforced state, i.e. without any loss in J_c. An
independent development is the use of magnetic materials, as Incoloy,
having the same thermal expansion coefficient as Nb_3Sn.

6.2.2 Facilities at KfK

A problem arising in NET-like conductors is how the different
components, e.g. steel, Cu (the ratio $Cu:Nb_3Sn$ is quite high, > 3:1
in Table 2.3-1), CuNi and the soldering operation at $\sim 200°C$ will
influence the value of J_c as well as its strain sensitivity. The
answer can only be given by J_c vs. ε measurements on these
conductors.

An unique measuring device has been developed at KfK for measuring
J_c vs. ε up to forces of 10 kN, currents of 3000 A and magnetic
fields of 14 T on wires with cross sections up to 30 mm^2. A 5 kN
strain rig /26/ is schematically represented in Fig. 6.2-4. In the 10
mm gap, fields up to ~ 14 T can be reached. The 10 kN, 3000 A strain
rig (see first results in 6.3) is 19 mm thick instead of 9 mm. In a
20 mm gap, the J_c vs. ε measurements can be performed up to
12.7 T.
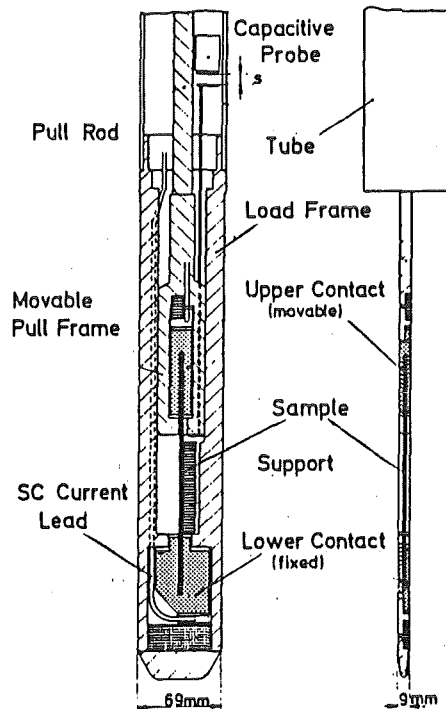
Fig. 6.2-4: The 5 kN, 1500 A strain rig /26/.

Actually, an even larger strain rig is under construction, with the
design values 100 kN and 10 kA. This device will be used for charac-
terizing subscale NET conductors with cross sections well above
200 mm^2 up to 14 T.

6.3   Fabrication of conductors on the basis of Nb$_3$Sn strands

The realization of the future NET conductor requires practical ex-
perience of the individual fabrication steps. To cover this point KfK
started an appropriate programme to investigate the relevant fabrica-
tion steps, necessary during the assembly of the NET-conductor. It
was thought that the best way to learn as much as possible on the
industrial feasibility of such large size complex conductors was to
fabricate various subsize models, showing at least one NET-relevant
point each. In the following the Nb$_3$Sn subsize conductor Model NR is
briefly discussed (see Fig. 6.3-1).
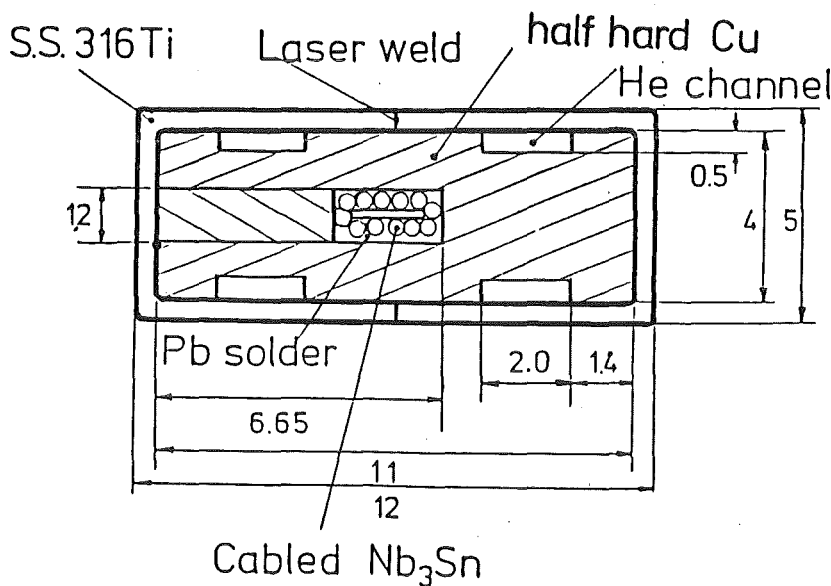
Fig. 6.3-1: A subscale conductor (12x5 mm^2 cross section) with
            NET-like configuration, actually tested at KfK (NR)
            (7 Nb$_3$Sin strands and 5 Cu wires, Ø 0.4 mm).

6.3.1 Description of the individual elements

- Nb_3Sn Superconducting cable

  This is a commercially available A15 superconducting cable, composed of 12 strands, five strands of stabilizing copper and 7 strands of bronze processed Nb_3Sn wire. The strand dimension is 0.4 mm. The 12 strands are cabled on a stainless steel core of 0,25 x 1,8 mm, thus giving a cable of 2,5 x 0,9 mm.

- Copper block

  The copper block is chosen as a mechanical stiffener. It shall also simulate the electrical stabilization and the cooling channels. It is drawn to the required dimension on a standard draw bench (lengths of $\sim$ 5000 mm). The helium channels and the Nb_3Sn cable slit were prepared by machining. It is possible to draw such a shape stepwise, but for the short test pieces it seemed to be more economical to use the machining process.

- Conduit

  The conduit of the conductor is fabricated with two U-profiles of the material AISI 316 Ti (German Werkstoff Nr. 1.4571). The U-profiles were completed within the common industrial practice (DIN 17.118 and DIN 59.413) with guiding and folding rolls in lengths of $\sim$7000 mm.

6.3.2 Assembly of the elements to a conductor

The length of the finished conductor was fixed to be $\sim$ 500 mm. This length was the minimum necessary size to measure I vs. $\mathcal{E}$ in magnetic field environment of $\sim$13 Tesla. The assembly began by cutting the Nb_3Sn cable in pieces of 500 mm length and placing them between SS jacks. The protection against sticking was achieved by means of commercial available ceramic band foils.

The reaction to Nb_3Sn was performed under high vacuum and 100 h at $700\,^{\circ}C$. The slit in the copper block was cleaned with solder flux and a layer of solder was processed in the slit by indirect heating. The reacted Nb_3Sn cable was inserted into the slit which was finally filled with solder at $220\,^{\circ}C$. The two U profiles were cleaned and placed in the weld position in a special gripping arrangement.

The main requirements for the 0.5 mm thick weld joint are given in the following:

- A weld process with minimum heat input, thus without any damage of the already soldered section (temperature rise in solder during the welding should be less than the melting point of the solder).
- A weld process with minimum distortion of the conductor shape after welding
- sound and helium tight weld seam.

According to the above requirements the laser weld process is the most suitable one, because of its high energy density and low heat input in the adjacent material. The melting of solder joint during welding limits the classical TIG welding process.
The results of the first laser weld procedure can be summarized in the following:

- Nd-Yag — 120 W laser working equipments are able to weld the 0.5 mm thick stainless steel conduit. But the process itself with 0.1m/min welding speed is too slow for a later industrial adoption
- CO_2-laser processing in continous wave mode seemed to be the most suitable one
- Sound welds could be achieved with a CO_2-laser working station of 3 kW capacity. The optimal beam power was 1500 Watts. The welding speed was in this case 6 m/min. This high speed resulted in low heat input with negligible temperature increase of the materials copper and Nb_3Sn core. Precise guiding rolls to keep the material motion in exact position and clean conditions are a top requirement to achieve helium tight weld seams.
- The conduit of NET-II type conductor is weldable by laser beams with 2-3 kW working power. Material thickness in this case will be ~2-3 mm and therefore need of such high beam power is necessary
- In actual production a subdivision of the laser beam from one working station is possible. Simultaneous welding of two or four weld seams with one station is the common standard
- The conduit of NET-II type conductor with its 2.45 mm thickness (~3 mm weld penetration) and I-type joint is only weldable by laser beams (not considering the EB welding process) and the associated vacuum problems).

6.3.3 <u>Test of conductors</u> Different qualification tests on conductors are a primary need prior to the end design of the coil. For the establishment of engineering data following tests can be done in the already existing facilities at KfK:

- Uniaxial stress vs. strain
- Bending tests parallel and perpendicular to the wide side of the conductor
- Fatigue response of the winding pack (insulation damage)
- Compressive tests on conductors and conductor packs with different grouping of the conductors. Modulus determination. Hysteresis of stress vs. strain
- Lap joint tests of stabilizing copper
- Helium tightness
- Mechanical behaviour of the weld zone
- Uniaxial strain vs. J_c in magnetic field
- Compression of the conductor and its strain vs. J_c behaviour in magnetic field
- Conductor ac losses
- Helium flow response of the conductor
- Conductors degradation after the various fabrication steps (handling)
- Response to neutron and gamma irradiation
- Quality assurance development
- Insulation tests.

6.3.4 <u>Critical current measurements on the 12 x 5 mm^2 subscale conductor</u>

The Nb_3Sn conductor represented in Fig. 6.3-1 was measured under two different aspects, without the external steel conduit (NR0, 4x11 mm^2) and with the steel conduit (NR1, 5x12 mm^2) after a reaction of 64 hours at 700^oC. A comparison of the critical current values (Fig. 6.3-2) shows no essential difference between 6 and 12 T. The Kramer plots yield B^*_{c2} = 19.8 T, i.e. 1 T less than for Nb_3Sn wires. The conductor NR1 shows slightly larger I_c values below 6 T, which is not understood, but is rather irrelevant. This could be correlated to the fact that the conductor NR1 was annealed 20 minutes at 500^oC in order to soften the Cu. This operation was rendered necessary by the limited force of the actual tensile machine, i.e. 10 kN. After this

heat treatment, the highest measured strain at 10 kN was 0.43% (see Fig. 6.3-3). The uncertainty is of the order of $\pm$ 0.1%, and will be lowered in the future by using improved strain gauges, in particular capacitive gauges, which are field-independent.

From these first measurements on conductors with such large cross sections (it should be noted that the total cross section of 60 mm^2 is small with respect to NET dimensions, but is rather large for J_c vs.ε measurements), the following conclusions can be drawn:

a)   Adding an external steel conduit after reaction by laser welding two U profiles does not affect J_c in the range between 6 and 12 T.

b)   The value of J_c (max) was not attained with the present tensile machine, in spite of the measured strain of 0.43 $\pm$ 0.1%. This means that the precompression is slightly enhanced with respect to the original Nb_3Sn + bronze and Cu or Cu + Steel.
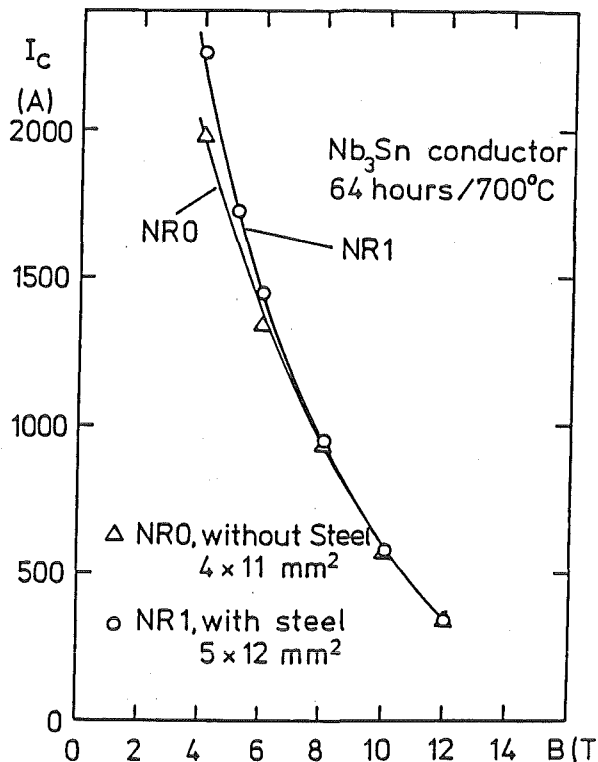
Fig. 6.3-2: J_c vs.B for the subscale 12 x 5mm^2 Nb_3Sn conductor with and without steel conduit
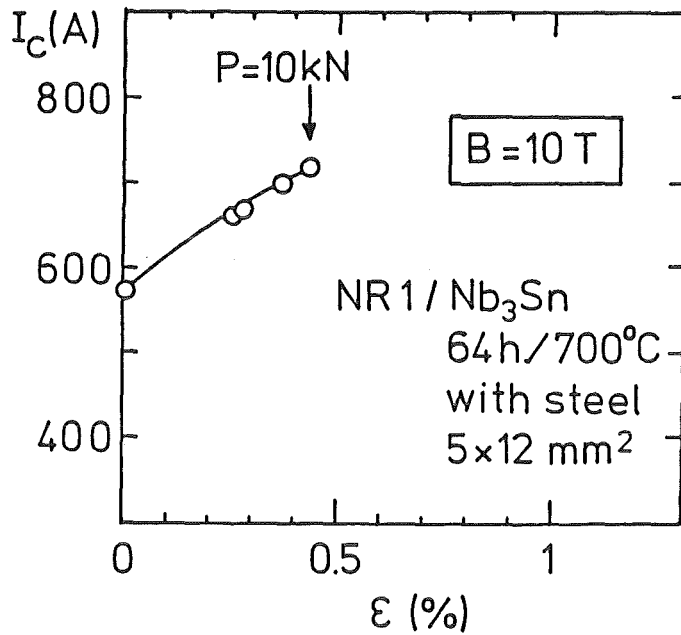
Fig. 6.3-3: J_c vs. ε of the 12 x 5 mm^2 subscale Nb$_3$Sn conductor with the steel conduit (NR).

A correct interpretation of these results needs further measurements on the initial wires and on the Nb$_3$Sn cable without Cu. Nevertheless, these first experiments demonstrate the usefulness of measuring J_c vs. ε for characterizing even complex Nb$_3$Sn conductors. It is remarkable that the applied strain caused an increase of J_c from 575 to 717 A, i.e. 24%, which is markedly higher than the values measured by Ekin at 10 T /31/. This shows the expected effects after bending or after transversal force application will be considerable.

6.4 Investigations on heat transfer and thermo-hydraulics

The thermo-hydraulic operational conditions of a Nb_3Sn Sn coil differ in several aspects from that of NbTi which have been studied intensively during the development of the forced flow cooled LCT coils. Some of those differences are:

- Higher possible operational temperatures. This permits the operation in such a pressure/temperature range where frictional pressure drop is associated with temperature drop. This range, however, is close to the transposed critical line of the coolant. Here, the data of heat transfer and coolant flow are rather shaky.
- Higher heat flux during stabilization. The deviation of heat transfer models from conventional correlations proves to be an important parameter for the design of the conductor and of the coil. More reliable data are necessary.

To make those effects and others better predictable, they should be studied more detailed in configurations which are relevant for large coils.

Mainly two test facilities are available for such investigations. The HELITEX facility has been used for the thermohydraulics studies of the LCT coils /2/. This set-up is shown in Fig. 6.4-1 and the main parameters are listed in Tab. 6.4-1. This facility can be used for various investigations such as

- simulation of the whole test loop including pumps, heat exchangers and control units
- evaluation of the friction loss at operational conditions
- thermohydraulics stability
- cool down
- quench pressure.

More detailed investigations on heat transfer will be done with a new apparatus, HeIIP/FF-Kryostat. This apparatus has been designed mainly for heat transfer investigations of forced flow superfluid helium

HeII). But it can also be operates at higher pressure and temperature conditions, namely close to the transposed critical line. The dimensions of the samples to be tested may of about 0.2 m diameter and 1 m height. Flow rates of about 1 g/s and cooling powers up to 10 W are available.

Furthermore, computer studies on forced helium flow with transient heat loads will be continued. The programme YAQHEL /2/ has been developed for such purposes. It will be modified to describe the conditions of the coil under consideration.
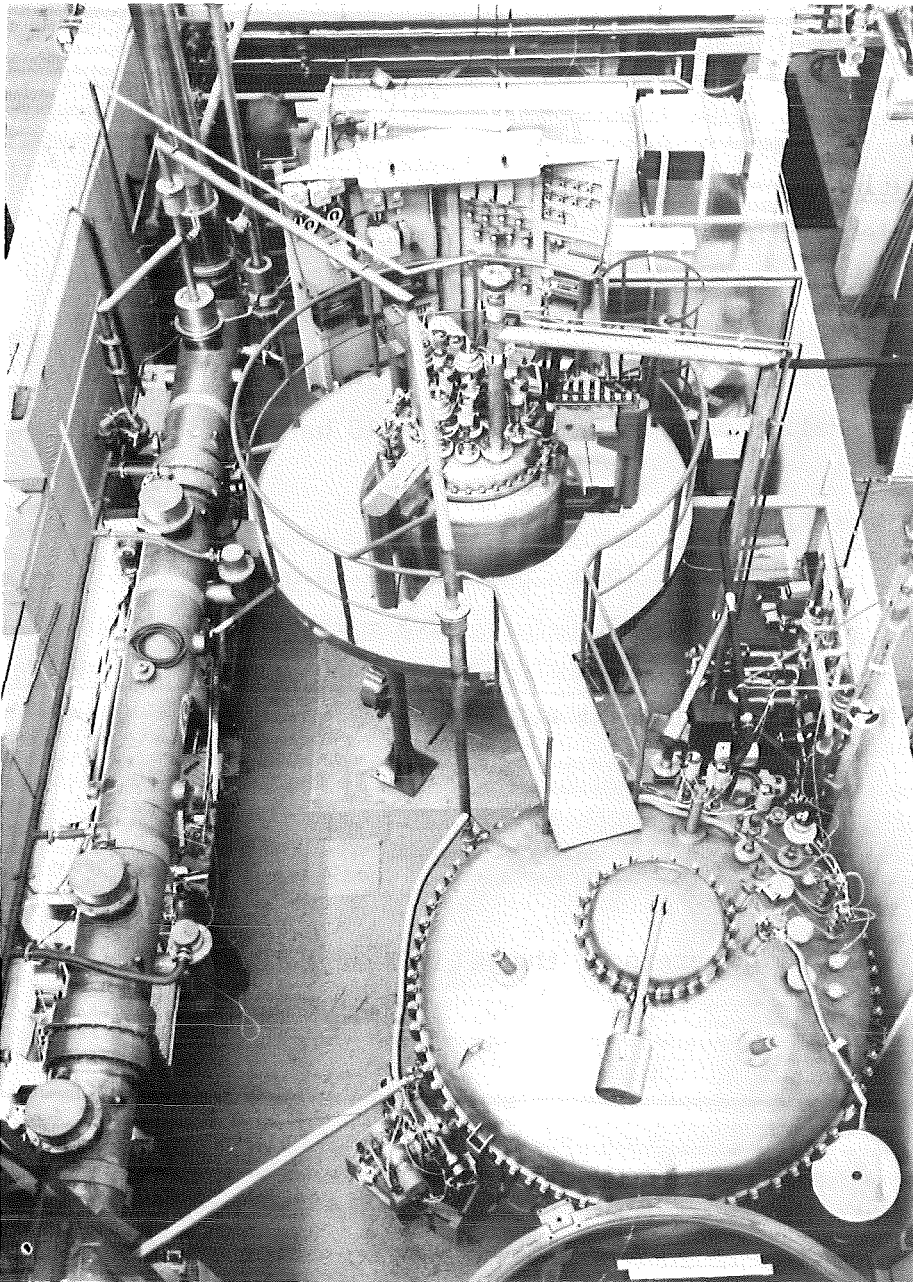
Fig. 6.4-1: The forced flow test facility, HELITEX.

Control dewar

Inner diameter	1050 mm
Height	2580 mm
Volume	1500 l
LHe content	850 l
Max. pressure	6 bar

Object cryostat

Inner diameter	2500 mm
Height	2450 mm

Operational parameters

Temperature	1.8 - 300 K

Pressure

Refrigerator loop	1 - 20 bar
Helium pump loop	1 - 10 bar

Mass flow rate

Refrigerator loop	0.5 - 20 g/s
Helium pump loop	0.5 - 150 g/s

Maximum heat load at 4.2 K   300 W

Tab. 6.4-1: Parameters of the HELITEX test facility

Conclusions

A Nb_3Sn conductor for NET-II TF coils with a maximum field at the coil
winding up to 11 T has been designed.
Starting point for the conductor concept was the design philosophy for NbTi
TF conductors, well proven by the Euratom/LCT coil in all conductor tests
and the domestic tests of the coil. Its principles are forced flow cooling,
large wetted perimeter for a given hydraulic diameter (to provide optimal
stability), mechanically fixed strands (to avoid micromovements), strand
separation (for small a.c. losses) and steel reinforcement (for hoop stress
support).

A conductor concept based on these principles but taking into account the
pecularities of Nb_3Sn was developed for a rated current of 20 kA at 12 T. It
consists of a flat Nb_3Sn cable, soldered to a surrounding CuNi tape after
reaction. Around this rectangular conductor core Cu profiles are cabled on
distance by the Roebel-process and subsequently soldered at the bottom onto
the CuNi tape. The whole system is surrounded by a steel conduit. The
present conductor data results from electric, thermohydraulics and stability
calculations as well as mechanical evaluations and takes into account
nuclear heat. Expected fabrication processes are discussed too. The
fabrication should be possible within the capabilities in European industry.
A cost estimate for the conductor indicates that the specific costs of a
NET-II 12 T conductor (per Ampere x meter x Tesla) are very similar to those
of the LCT conductor.

References

/ 1/   Intor Phase II A Report IAEA, 1983

/ 2/   G. Krafft, Proc. 8th Int. Cryo. En. Conf. Genova, 3-6 June, 1980,
       p.754

/ 3/   C. Schmidt: "Critical current, stability and ac loss measurement on
       the EURATOM-LCT-Conductor"; IEEE Trans. Magn., MAG-19 (1983), pp. 707

/ 4/   W. Herz et al.: "Results of the Test of the European LCT coil in the
       TOSKA Facility"
       IEEE Trans. Magn., MAG-249, (1985)

/ 5/   A. Nyilas, private communication

/ 6/   This information has been given by Vacuumschmelze

/ 7/   W. Maurer, Neutron Irradiation Effects on Superconducting and
       Stabilizing Materials for Fusion Magnets. KfK 3733, May 1984

/ 8/   W. Maurer, Neutron and Gamma Irradiation Effects on Organic Insulating
       Material for Fusion Magnets, to be published as KfK report.

/ 9/   W. Daenner, Neutronics results for superconducting coils,
       NET/IN/84-067

/10/   C.L. Snead et al., J. Nucl. Mater., 103 & 104, 749 (1981)

/11/   V. Arp, Adv., Cryo. Eng., 17 (1972), 342-351

/12/   W. Stautner, unveröffentlichter Bericht (1981)

/13/   R.D. McCarthy, Thermophysical properties of Helium-4 from 2 to 1500 K
       with pressures to 1000 atmospheres, NBS Technical Note 631 (1972)

/14/ B.A. Hands, HEPROP - A computer code for the thermodynamic and thermo-
     physical properties of helium - Third Edition Oxford University, Eng.
     Lab. Department Report 1289/79 (1979)

/15/ P.J. Giarratano, V. Arp, and R.V. Smith, Cryogenics 11 (1971) 385

/16/ V.M. Yeroshenko and L.A. Yaskin, Cryogenics 21 (1980) 94

/17/ P.J. Giarratano and M.C. Jonses, Deterioration of heat transfer to
     supercritical helium at 2.5 atm., Int. J. Heat Mass Transfer, 1975,
     649-653

/18/ M.C.M. Cornelissen and C.J. Hoogendoorn, Turbulent heat transfer to
     supercritical helium. A numerical study, Proc. of the Int. Congr. of
     Refrig. (IIR), Commission B1, A1/2, Paris 1983

/19/ N.M. Schnurr, Numerical prediction of heat transfer to supercritical
     helium in turbulent flow through circular tubes, Trans., ASME, 99
     (1977), 580-585

/20/ J.R. Miller et al., Proc. 8th Int. Cryog. Eng. Conf. Genova,
     3-6 June, 1980, p. 321

/21/ V.B. Zenkevitch, A.S. Romaniuk, Losses in multifilamentary supercon-
     ductors of low levels of exitation, IEEE Trans. on Magn., Vol. MAG-13,
     Jan. 77

/22/ P.E. Daney, P.R. Ludtke, and M.C. Jones, "An experimental study of
     thermally-induced flow oscillations in supercritical Helium", J. Heat
     Transfer, 101, 9 (1979)

/23/ E. Drost, R. Flükiger, and W. Specking, "Superconducting and metallur-
     gical properties of bronze processed Nb_3Sn wires with Ta, Ti and Ni+Z
     additions", Cryogenics, 24, 622 (1984)

/24/ E. Drost, W. Specking, and R. Flükiger, "A comparison of critical current densities and electrical resistivities in Ta, Ti and Ni+Zn alloyed Nb$_3$Sn wires up to 24 T", IEEE Trans. Magn., MAG-21, 281 (1985)

/25/ R. Flükiger, E. Drost, and W. Specking, "Effect of internal reinforcement on the critical current density of Nb$_3$Sn wires", Adv. Cryo. Eng., Vol. 30, 875 (1984)

/26/ W. Specking and R. Flükiger, "A compact 5 kN test facility for super-conducting conductors carrying up to 1.5 kA in magnetic fields up to 14 T", J. Physique, 45-C1, 365 (1984)

/27/ J. Benkowitsch and G. Krafft, "Numerical analysis of heat-induced transients in forced-flow helium cooling systems", Cryogenics, 20, 209 (1980)

/28/ S.C. Sackett, "EFFI, A code for calculating the electromagnetic field, force and inductance in coil systems of arbitrary geometry", LLNL, Livermore, CA, UCRL-52402 (1978)

/29/ P. Turowski, to be published

/30/ Information from manufacturer (Krempel, Stuttgart)

/31/ J. Ekin, IEEE Trans. Magn., MAG-17, 658 (1981)